Electrical Response of Materials Containing Space Charge with Discharge at the Electrodes

J. Ross Macdonald
Texas Instruments Incorporated, P.O. Box 5936, Dallas, Texas 75222
(Received 7 October 1970)

The system considered consists of a solid or liquid material containing mobile positive and negative charges between two identical plane electrodes separated by a distance l. The results obtained apply also for a single working electrode, without specific adsorption, and an indifferent electrode. Uni-univalent, nonrecombining positive and negative charges, usually of equal mobility, are assumed. Frequency and transient responses are compared in the linear regime for two different boundary conditions. One condition requires complete blocking of positive and negative charges at the electrodes; the other requires complete blocking for charges of one sign but allows free discharge of those of opposite sign. The working electrode is thus reversible, or Ohmic, for charges of one sign. The method of solution includes electromigration effects, does not require electroneutrality anywhere, and leads to results satisfying Poisson's equation exactly everywhere for all times and frequencies. These results apply to solids and liquids with either electronic or ionic conduction. They are relevant to low-conductivity liquids, as in Kerr and liquid-crystal-display cells, to ordinary solid and liquid electrolytes, and at least to some extent to fused salts. Although the frequency and transient responses involve continuous distributions of relaxation times, three main relaxation times, τ_D, $M\tau_D$, and $M^2\tau_D$, occur. Here τ_D is the dielectric relaxation time of the charge-containing material and $M\equiv l/2L_D$, where L_D is the appropriate Debye length. Results are obtained for any value of M but are summarized here for the usual experimental condition $M\gg1$. At high normalized frequencies, $\Omega\equiv\omega\tau_D\gg1$, the system parallel capacitance associated with mobile charge is proportional to $\omega^{-3/2}$ for both blocking and discharge conditions. The series capacitance is proportional to $\omega^{-1/2}$ for these conditions. It is shown, for the first time in the completely blocking situation, that this high-frequency response is associated with a Warburg, or diffusion, impedance. An equivalent circuit is obtained for the discharge case with a maximum of frequency-independent elements and a minimum frequency dependence of remaining elements. It involves a dc path and two distinct Warburg impedances, occurring in different frequency ranges. Cole–Cole plots of the effective complex dielectric constant associated with the "interface" elements of the equivalent circuit yield, for both boundary conditions, curves very close to that arising from a Davidson–Cole continuous distribution of relaxation times with distribution parameter $\beta=0.5$. In the limit of large M, blocking frequency response becomes identical with such Davidson–Cole response. Interface transient response is found in both cases to involve regions where the current decay is proportional to $t^{-1/2}$, but that in the discharge case can occur over a very long time range extending to $t\sim5\times10^{-4}\,M^2\tau_D$. For large M, this limiting time may be measured in days or months. The long-time limit of the transient charge is finite and consistent with the low-frequency limiting capacitance of the system. Although the $\Omega\to0$ space-charge capacitance in the blocking case is independent of l, the corresponding dominant capacitance in the discharge case is extrinsic and directly proportional to l, making potentiostatic measurements inapplicable at very long times. It is about $M/12$ times larger than the blocking-case capacitance and arises from charge diffusion (not space charge) in a finite length, the entire bulk region. Tremendously large capacitances may thus appear at ultra-low frequencies since M may often be as large as 10^6. Some applications and limitations of the present results to electrolyte situations are discussed, and the important effects of a finite l are emphasized. Faradaic and non-Faradaic processes do not separate clearly in the present discharge case, but it is suggested that when an excess of indifferent electrolyte is present in addition to the discharging ion such separation may be a good approximation. An approximate equivalent circuit is proposed for this situation which differs in important ways from those heretofore employed by electrochemists.

I. INTRODUCTION

In 1953 an exact, closed-form expression was given for the admittance of a charge-carrying liquid or solid between two plane, parallel, completely blocking electrodes.[1] This one-dimensional treatment applies for arbitrary ratio of the mobilities of uni-univalent charge carriers present and for an arbitrary degree of ionization of a charge carrier of a given sign from a recombination center. This work was followed shortly thereafter by Friauf's[2] treatment of a similar situation involving somewhat more general boundary conditions at the electrodes. Following Chang and Jaffé,[3] Friauf assumed that the positive and negative carriers (of equal equilibrium bulk concentration, c_0) could discharge at the electrodes to a degree determined by blocking, or discharge, parameters, r_p and r_n, separately specified for each sign of carrier. Although Friauf gave closed-form expressions for the over-all current in his analysis, he did not derive and investigate expressions for parallel capacitance and conductance holding for all frequencies. Instead he gave some formulas pertinent in limited (but unspecified) frequency ranges and presented a few calculated curves appropriate for various boundary conditions such as positive carriers free ($r_p=\infty$), and negative ones blocked ($r_n=0$) [termed the $(\infty,0)$ case by Friauf].

Finally, Beaumont and Jacobs[4] have investigated the situation of completely dissociated, mobile negative carriers with adjustable discharge at the electrodes. Here, unlike the Friauf $(\infty,0)$ case mentioned above, the negative charges arise from complete ionization of neutral centers taken uniformly distributed throughout the material. The resulting positive charges are thus

fixed in position and do not discharge. Friauf's[2] and the author's[1] analyses, where positive and negative charges may both move, are applicable to either liquids (electrolytes and low conductivity dielectrics) or homogeneous solids, while the Beaumont–Jacobs results apply only to solids. The present treatment and the others cited above only apply, as usual, for small applied sinusoidal voltages, appreciably less than kT/e in magnitude. Here k is Boltzmann's constant, T the absolute temperature, and e the protonic charge.

Friauf's analysis yielded $\omega^{-3/2}$ frequency dependence for his parallel space-charge capacitance in the $(\infty, 0)$ and $(0, \infty)$ partial discharge cases. Here $(0, \infty)$ designates positive charges blocked, negative ones free. Such frequency dependence differs significantly from the usual limiting ω^{-2} single-time-constant Debye behavior found both for completely blocking electrodes[1,5] (any mobility ratio) and for the Beaumont–Jacobs[4] situation of a mobile charge carrier of a single sign with arbitrary discharge. Friauf[2] and several later writers[4,6–9] have, therefore, frequently taken experimental observation of approximate $\omega^{-3/2}$ behavior to indicate the presence of discharge of one type of carrier and blocking of that of the opposite sign.

A recent new analysis[10] for the $(0, 0)$, completely blocked, situation[1] with equal mobilities has uncovered the somewhat surprising result that this case too leads to $\omega^{-3/2}$ behavior for the parallel capacitance of exactly the same magnitude as that given by Friauf in the $(0, \infty)$ or $(\infty, 0)$ cases. This behavior appears for the $(0, 0)$ case, however, only at extremely high relative frequencies ($\omega\tau_D \gg 1$), beyond the Debye region. Accurate measurements in this region are usually difficult and even those near $\omega\tau_D = 1$ may be. Here τ_D is the dielectric relaxation time of the charge-containing material and is an intrinsic, not extrinsic, property of the material considered. It can range from more than a second for high resistivity solids and liquids to less than 10^{-9} sec for high conductivity electrolytes. We shall frequently hereafter use the normalized frequency variable $\Omega \equiv \omega\tau_D$. For $\Omega < 1$, usual Debye response was found in the $(0, 0)$ case.

The above agreement in frequency dependence with the different Friauf discharge case suggested to me that Friauf's $\omega^{-3/2}$ dependence might also apply only for $\Omega \gg 1$. Since his unnormalized parallel capacitance curves showed no deviation from $\omega^{-3/2}$ behavior, it was impossible to determine the Ω range they covered by inspection, and the applicability of the $\Omega \gg 1$ condition could not be readily tested.

Clearly, if completely blocking and partial discharge situations both led to identical $\omega^{-3/2}$ behavior only in the same high-frequency region, actual experimental observation of such dependence would not allow one to distinguish between the two cases. The above results indicated that a more complete comparison between results for the $(0, \infty)$ and $(\infty, 0)$ situations and those for the $(0, 0)$ case would be of value, In addition, I felt it important to discover for these cases the equivalent circuits which represent them in the simplest way with a maximum of entirely frequency-independent resistive and capacitative elements and minimum frequency dependence of any remaining elements. Such minimax circuits yield, I believe, the simplest physical interpretation of the processes occurring in the material considered.

The present general area has been treated in the past independently from their own special viewpoints by solid state physicists and chemists and by electrochemists. The present work is in part an attempt to join together the previously rather uncoupled viewpoints and methods in these fields. It leads to a number of new conclusions concerning the behavior of solid and liquid electrolytes and emphasizes the extreme response changes which can occur when a blocking electrode becomes even somewhat discharging.

II. PRELIMINARY ANALYSIS

In comparing the blocking and partly discharging cases, I have for simplicity considered uni-univalent, nonrecombining charge carriers of equal mobility. In this equal mobility situation there is, of course, no difference between the $(0, \infty)$ and $(\infty, 0)$ end results. In the comparison I use the results of the recent $(0, 0)$ calculations[10] and, rather than employ Friauf's own rather complicated formulas, I have applied the straightforward methods of Ref. 1 to obtain a closed-form admittance for the $(0, \infty)$ case using the Chang–Jaffé discharge boundary conditions. In this case, they reduce to (a) the usual expression for zero positive-carrier convection current at the electrodes and (b) no perturbation of the negative charge carrier concentration at the boundaries from its (assumed) initial homogeneous, equilibrium value, c_0. This quantity is also the equilibrium value of the positive charge concentration in the absence of space charge.

In the present analysis, inner-layer complications and specific adsorption are ignored; no supporting electrode is present; and results apply exactly only at the point of zero static electrode charge. Discussion of these restrictions and some relaxation of some of them appears in the final section.

Both blocking and discharge solutions are obtained by solving,[1] in the linearized approximation, the usual idealized transport and Poisson equations exactly everywhere for positive and negative charge. In this sense, the analysis is a microscopic one. It does not apply exactly to intrinsic semiconductors or to charged vacancies in solids since complete dissociation of charges is assumed. Insofar as the boundary conditions used are met in these situations, however, it should nevertheless apply fairly closely.[1] The analysis should certainly apply to ionic motion in solids and liquids and should include the situation of dielectric materials with very low conductivity arising from the presence of a small concentration of ionized impurities.

In order to define the response of the system to a sinusoidal signal, both parallel and series quantities are

useful and will be distinguished by a subscript "P" or "S." Admittances will be generally taken as involving parallel elements and impedances, series elements. For convenience I shall, however, use both parallel and series conductances. The inverse of a series conductance is, of course, a series resistance. A subscript "zero" will generally denote a $\Omega\rightarrow 0$ limiting value, while an "infinity" subscript will denote a value appropriate when $\Omega\gg 10$. Finally, an "N" added to a subscript indicates that the quantity in question has been normalized with the real part of its $\Omega\gg 10$ value if it is an immittance (impedance or admittance), conductance, or resistance, or its $\Omega\rightarrow 0$ value if it is a capacitance. The same "N" subscript also denotes a normalized charge or current. Since I shall always be considering unit area herein, I shall frequently make no distinction between such quantities as capacitance/unit area and capacitance, current density and current, etc.

The total admittance/unit area, Y_T, of the material between plane, parallel electrodes separated a distance l apart may be written for the $(0, \infty)$ discharge case as

$$Y_T = G_T + i\omega(C_g + C_P), \tag{1}$$

where clearly G_T and (C_g+C_P) are electronically in parallel. Here $i\equiv(-1)^{1/2}$, and C_g, the geometrical capacitance/unit area, is equal to $\epsilon/4\pi l$; it arises from polarization of the underlying material (dielectric constant ϵ) containing the mobile space charge. Thus, C_g will generally be frequency independent over the range where space charge leads to frequency dependence of the parallel quantities G_T and C_P. Finally, it is desirable to define the high-frequency limiting bulk conductance/unit area, G_∞, and the Debye length, L_D. For the present equal mobility situation, $G_\infty = 2e\mu_n c_0/l$ and $L_D = [\epsilon kT/8\pi e^2 c_0]^{1/2}$. Here μ_n is the mobility of the negative charge carrier. The dielectric relaxation time, τ_D, is defined as $\epsilon/4\pi\sigma_\infty$, where $\sigma_\infty \equiv lG_\infty$ is the high-frequency conductivity of the material. Hence, in the present case of two parallel electrodes, $\tau_D = C_g/G_\infty$, independent of l. Note, that the important condition $\Omega\equiv\omega\tau_D = 1$ defines the frequency for which the susceptance/unit area, ωC_g, of C_g equals the conductance/unit area, G_∞. For future use let $M\equiv l/2L_D$ and $r\equiv M\,\mathrm{ctnh}(M)$.

Let us now separate Y_T into a part involving frequency-independent elements, Y_C, and a frequency-dependent space-charge remainder, Y_P. Analysis shows that G_T reaches G_∞ in the limit of high frequencies $(\Omega\gg 1)$ and goes to $(G_\infty/2)$ as $\Omega\rightarrow 0$. This $G_\infty/2$ must equal $\mu_n e c_0/l$ (as opposed to the equal $\mu_p e c_0/l$) in the limit of zero frequency since only negative charge carriers can discharge in the $(0, \infty)$ case. The only current passing into an electrode in this limit, the negative carrier convection current, can be calculated directly for $\Omega\rightarrow 0$ and yields $-(\mu_n e c_0/l)\,V_1$, where V_1 is the amplitude of the applied sinusoidal potential. It is defined such that the left electrode $(x=0)$ is positive for $V_1>0$.

We may now write $Y_T\equiv Y_C+Y_P$, where $Y_C\equiv(\mu_n e c_0/l)+i\omega C_g$, and $Y_P\equiv G_P+i\omega C_P$. Thus, $G_P\equiv G_T-(\mu_n e c_0/l)$ and is zero at $\Omega\rightarrow 0$. It is very important to emphasize that the removal of Y_C from Y_T is essential to allow one to define a space-charge Y_P which will lead to an impedance $Z_S\equiv Y_P^{-1}$ whose equivalent series resistance and capacitance are frequency independent over a maximum frequency range. The determination of such series elements is, of course, very desirable in establishing equivalent circuits and in physically interpreting measured admittances or impedances.

Although the $\mu_n e c_0/l$ conductance that is removed to obtain G_P derives only from the negative carriers and is frequency independent, the actual negative carrier convection current magnitude evaluated at the $x=0$ electrode, $j_{n_1}(0)\equiv e[\mu_n c_0 E_1(0)+D_n(dn_1/dx)_0]$, is only equal to $-(\mu_n e c_0/l)\,V_1$ for $\Omega\rightarrow 0$. Here $E_1(0)$ is the electric field amplitude at this electrode, $(dn_1/dx)_0$ is the negative carrier concentration gradient evaluated at the same electrode, and D_n is the negative charge carrier diffusion coefficient. The current $j_{n1}(0)$ thus involves a purely conductive term only in the limit of zero frequency and includes reactive components otherwise.

Now define the normalized space-charge admittance $Y_{PN}\equiv Y_P/(G_\infty/2)$. We shall usually not distinguish between $\mu_n e c_0/l$ and $\mu_p e c_0/l$ from now on since they are both equal to $G_\infty/2$ in the present equal mobility case. Straightforward analysis of the type employed in Ref. 1 leads for the $(0, \infty)$ situation to

$$Y_{PN} = 1 - \frac{2(1+i\Omega)}{1+iM\Omega(1+i\Omega)^{1/2}\,\mathrm{ctnh}[M(1+i\Omega)^{1/2}]+M(i\Omega)^{1/2}(1+i\Omega)\,\mathrm{ctnh}[M(i\Omega)^{1/2}]}. \tag{2}$$

Further,

$$G_{PN}\equiv G_P/(G_\infty/2) = \mathrm{Re}(Y_{PN}), \tag{3}$$

$$C_P/C_g = (2\Omega)^{-1}\,\mathrm{Im}(Y_{PN}). \tag{4}$$

Analytic separation of Y_{PN} into real and imaginary parts leads to clumsy expressions which need not be given here. Computer calculation of space-charge capacitance and conductance dependence on Ω for a variety of M values has been carried out and allows easy comparison with corresponding $(0, 0)$ results. The quantities G_P and C_P are, of course, electrically in parallel. Previous work[1,10] has shown that equivalent series quantities tend to be frequency independent over much wider ranges of normalized frequency than those applying for G_P and C_P. Define the quality factor Q as $\omega C_P/G_P = [(C_P/C_g)/(G_P/G_\infty)]\Omega$. Then, the related series quantities are given by $C_S = (1+Q^{-2})C_P$ and $G_S = (1+Q^2)G_P$. The appropriate equivalent circuit will then

be made up of the frequency-independent C_g and $G_\infty/2$ in parallel and both in parallel with a branch containing the somewhat frequency-dependent elements C_S and G_S in series.

In the low-frequency limit, $C_P+C_g\rightarrow C_0$, the total directly measurable low-frequency capacitance. It will be convenient to normalize C_P and C_S with their common $\Omega\rightarrow 0$ value, (C_0-C_g). Let $s\equiv(C_0-C_g)/C_g$, $C_{PN}\equiv C_P/(C_0-C_g)=s^{-1}(C_P/C_g)$, and $C_{SN}\equiv C_S/(C_0-C_g)=s^{-1}(C_S/C_g)$. From (2) one finds that

$$s\equiv s_d=(M^2/12)+[(r-1)/4], \tag{5}$$

the important ratio of low-frequency capacitance to high-frequency capacitance in this case. Here the subscript "d" refers to the $(0,\infty)$ discharge case. For the present situation, Friauf found the less accurate result $s_d=(M^2/12)$, adequate when $M\gg 10$. Note that $2M$ is the number of Debye lengths contained in the electrode separation l; thus M is the number which is associated with a single electrode and half of the material between electrodes. The quantity M is a crucial, controlling ratio for the situations here investigated.

The $\Omega\rightarrow 0$ limiting expression for G_{PN} following from a lengthy calculation is, for the $(0,\infty)$ case,

$$G_{PN}\rightarrow\Lambda_d\Omega^2\equiv\tfrac{1}{2}(\Omega^2)\{\tfrac{1}{45}[M^2(M^2-15)]$$
$$+\tfrac{1}{2}[(M\ \mathrm{csch}M)^2-(r+1)]+\tfrac{1}{2}(\tfrac{1}{3}M^2+r)^2\}, \tag{6}$$

showing that G_{PN} depends on Ω as Ω^2 for sufficiently small Ω. In the completely blocking $(0,0)$ situation, $G_{PN}\equiv G_P/G_\infty$ [*not* $G_P/(G_\infty/2)$ as in the $(0,\infty)$ case] and is given by[10]

$$G_{PN}\rightarrow\Lambda_b\Omega^2\equiv\tfrac{1}{2}(\Omega^2)[3r(r-1)-M^2], \tag{7}$$

as $\Omega\rightarrow 0$. For large M, it is clear that the $(0,\infty)\Lambda_d$ coefficient of Ω^2 will be much larger than the $(0,0)\Lambda_b$ coefficient.

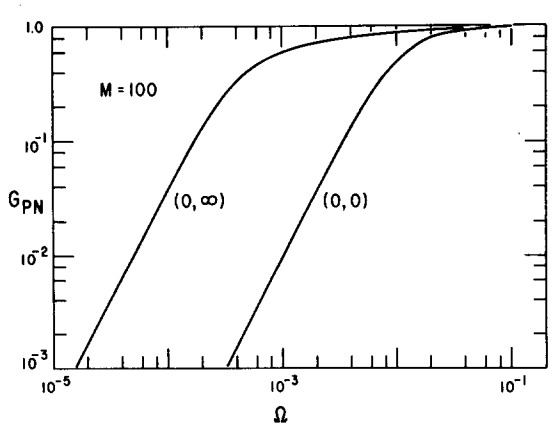

FIG. 1. $G_{PN}\equiv G_P/G_e$ vs $\Omega\equiv C_g\omega/G_\infty$ for $M=100$. Here $G_e=G_\infty$ for $(0,0)$ and $G_\infty/2$ for $(0,\infty)$.

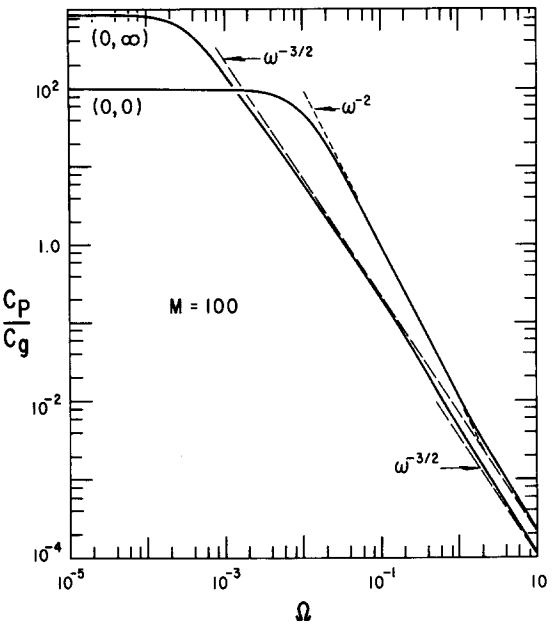

FIG. 2. C_P/C_g vs normalized frequency Ω for $M=100$ and the $(0,0)$ and $(0,\infty)$ situations.

III. INITIAL CALCULATED RESULTS

Calculated curves of G_{PN} for $M=100$ are presented in Fig. 1 and illustrate low-frequency limiting Ω^2 behavior. Although the graph cannot show it, there is a crossover of the normalized curves near $\Omega=0.05$, and at $\Omega=0.1$ values of G_{PN} are about 0.985 and 0.970 for the $(0,0)$ and $(0,\infty)$ cases, respectively. Remember, however, that different normalization is used in the two cases; thus the unnormalized curves do not cross.

The $\Omega\rightarrow 0$ limit of G_S, G_0, is readily calculated for the $(0,\infty)$ case and can differ appreciably from its high-frequency limit $(G_\infty/2)$. On normalizing G_0, one finds

$$G_{0N}=4s_d^2/\Lambda_d. \tag{8}$$

For $M\rightarrow\infty$, $G_{0N}\rightarrow(5/7)\cong 0.7143$. At $M=10^3$, 10^2, 10, and 1, G_{0N} is found to be about 0.7155, 0.7261, 0.7941, and 0.8367, respectively. G_{0N} approaches unity as $M\rightarrow 0$ and all space charge disappears. Thus, G_0 itself approaches $(G_\infty/2)$ as $M\rightarrow 0$. In the completely blocking situation on the other hand, one finds[1,10]

$$G_0\equiv(s_b^2/\Lambda_b)G_\infty\rightarrow(5/6)G_\infty$$

as $M\rightarrow 0$, and it increases rapidly toward G_∞ for $M>1$.

I shall return to series behavior later. Meanwhile, Fig. 2 illustrates the dependence of C_P/C_g on Ω for the two different boundary conditions and $M=100$. Note that as $\Omega\rightarrow 0$, C_P/C_g approaches $(C_0-C_g)/C_g\equiv s$. For the $(0,0)$ case, $s\equiv s_b=r-1$. Here, the actual $M=100$ values are 99 for $(0,0)$ and about 858.1 for $(0,\infty)$. Figure 2 shows usual Debye behavior for C_P/C_g in the $(0,0)$ case up to about $\Omega=1$; then there is a transition to the final limiting behavior already mentioned:

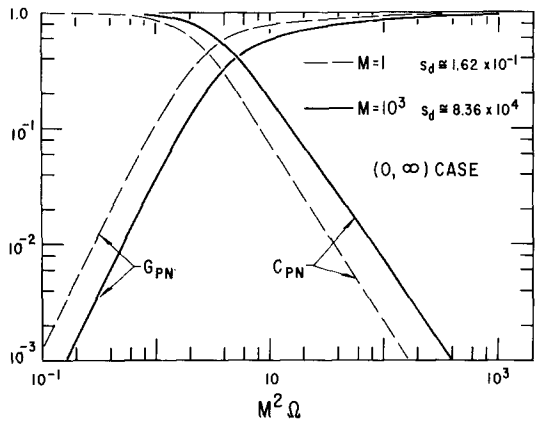

FIG. 3. G_{PN} and $C_{PN} \equiv C_P/(C_0 - C_g)$ vs $M^2\Omega$ for $(0, \infty)$ and $M = 1$ and 10^3.

$C_P/C_g \rightarrow \Omega^{-3/2}/\sqrt{2}M$ when $\Omega \gg 1$. This behavior is shown by the upper dashed curve. Since it does not occur until $C_P < C_g/M$, such limiting dependence will usually be very difficult to determine directly for $M \gtrsim 100$ or so. Remember that the total directly measured parallel capacitance is $(C_g + C_P)$. When $C_P < 0.01C_g$, for example, extraordinary accuracy in measuring $(C_g + C_P)$ will be required to allow $C_P \equiv (C_g + C_P) - C_g$ to be obtained with much accuracy of its own if C_P is derived from a parallel-circuit bridge balance. Other alternatives will be discussed later.

Friauf found the result $C_P/C_g = \Omega^{-3/2}/\sqrt{2}M$ also in the $(0, \infty)$ case. Analysis shows that his actual calculations of C_P vs ω curves employed an M value near 10^6, and he presented an $\omega^{-3/2}$ curve for C_P in the frequency range 50–5000 Hz. Clues in his paper suggest that 300 Hz corresponds to about $\Omega = 10^{-6}$. His actual calculations were carried out, however, for quite unequal mobilities. Nevertheless, it is clear that his formula and curve for C_P apply not as $\Omega \rightarrow \infty$ (i.e., for $\Omega \gg 1$) but in the region $\Omega \sim 10^{-6}$, or $M^2\Omega \sim 10^6$. We can now begin to sort out the $(0, \infty)$ situation. The appropriate curve of Fig. 2 shows that there is a region where $(0, \infty)$ C_P/C_g behavior approximates to $\Omega^{-3/2}/\sqrt{2}M$ (upper dashed line) and a further region beyond $\Omega = 1$ where the behavior is $\Omega^{-3/2}/2\sqrt{2}M$ (lower dashed line). Thus, for $\Omega \gg 1$ there is a factor of 2 difference in the $(0, 0)$ and $(0, \infty)$ C_P/C_g limiting curves. Further, for the $(0, \infty)$ case in the region $(10/M)^2 \lesssim \Omega \lesssim 0.1$, there is approximately $\Omega^{-3/2}/\sqrt{2}M$ behavior. In recent work,[10] I mistakenly compared this intermediate Friauf behavior with the final $\Omega \gg 1$ behavior found for the $(0, 0)$ situation. Incidentally this $\Omega \gg 1$ behavior will frequently be difficult to measure accurately because of such effects as electrode surface roughness, adsorption, parasitic elements, etc.

The $(0, \infty)$ case becomes clearer when we plot G_{PN} and C_{PN} vs $M^2\Omega$ rather than Ω, as in Fig. 3. We can now compare normalized curve shapes for various M's directly. Using this basic frequency variable, equal to $\omega l^2/4D_n$, we find that curves of practical interest are contained between those for $M = 1$ and $M = 10^3$ shown. There is little space charge present for $M \lesssim 1$ since $(C_0 - C_g)$ equals only about $0.16C_g$ at $M = 1$. Further, there is no appreciable change in shape for $M > 10^3$. For example, for $M^2\Omega = 1$, $G_{PN} \cong 0.0369$ at $M = 10^3$, 0.0368 at 10^4, and 0.0367 at $M \gtrsim 10^6$. For $M = 100$, it is 0.0383, and it reaches 0.0522 at $M = 10$.

If we now define a diffusion region length, l_d, as $(D_n/\omega)^{1/2}$, then $(M^2\Omega)^{1/2} = (\frac{1}{2}l)/l_d$. Thus, the variable $(M^2\Omega)^{1/2}$ measures the number of diffusion lengths contained in half the distance between identical electrodes. Since M is defined as $(l/2)/L_D$, a similar sort of ratio, one finds $\Omega^{1/2} = L_D/l_d$. When $\Omega = 1$, the diffusion length just equals the Debye length.

The reason for the remaining difference between $M = 1$ and $M = 10^3$ curves when $M^2\Omega$ is used as the frequency variable comes from the two different $\Omega^{-3/2}$ frequency ranges frequently present in the $(0, \infty)$ case. In Fig. 3, the entire part of the $M = 1$ C_{PN} curve of interest lies above $\Omega = 1$. Thus, only the final high-frequency limiting $C_{PN} = \Omega^{-3/2}/2\sqrt{2}Ms_d$ behavior appears. On the other hand, for $M = 10^3$, the C_{PN} curve shown includes only the beginning of the lower-frequency $\Omega^{-3/2}/\sqrt{2}Ms_d$ region appearing for $(10/M)^2 \lesssim \Omega \lesssim 0.1$. Thus the actual $M = 10^3$ curve shows a slope somewhat less than -1.5 and lies slightly below the above C_{PN} expression. The high-frequency $\Omega^{-3/2}$ region does not appear on the graph for $M = 10^3$ since $M^2\Omega$ would have to be $> 10^{12}$. Thus we see that it is the transition from the lower-frequency $\Omega^{-3/2}$ region to the upper limiting one as M decreases toward unity and below that causes the entire difference between C_{PN} curves plotted vs $M^2\Omega$. Note that both the $M = 1$ and $M = 10^3$ G_{PN} curves show Ω^2 dependence at $M^2\Omega < 1$.

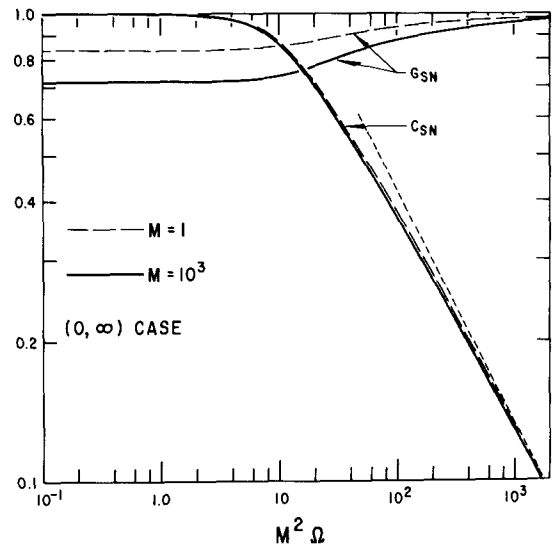

FIG. 4. $G_{SN} \equiv G_S/(\frac{1}{2}G_\infty)$ and $C_{SN} = C_S/(C_0 - C_g)$ vs $M^2\Omega$ for $(0, \infty)$ and $M = 1$ and 10^3.

Finally, it is of interest to examine the corresponding series quantities C_{SN} and $G_{SN} \equiv G_S/(G_\infty/2)$. Figure 4 shows their dependence on $M^2\Omega$. G_{SN} goes from G_{0N} to unity, with the main transition near $M^2\Omega \gtrsim 10$. Further C_{SN} stays reasonably constant for $M^2\Omega \lesssim 10$. Note that here the $M=1$ and $M=10^3$ curves for C_{SN} can scarcely be distinguished. At $M^2\Omega = 10^2$, the $M=1$ value is about 0.379 while the $M=10^3$ value is about 0.3682. For $M = 10^6$, the value is scarcely different, namely 0.3685. The dotted straight line is a limiting line given by $(3/M)(2/\Omega)^{1/2}$, appropriate for $M \gtrsim 10^2$, and corresponds to the first (lower frequency) $\Omega^{-3/2}$ region of C_P/C_g. Thus, for M values of usual interest the basic normalized quantities C_{SN} and G_{SN} are effectively functions only of $M^2\Omega$ in this frequency region, *not* of M and Ω separately.

IV. EQUATION SUMMARY

We have seen that in both the $(0, 0)$ and $(0, \infty)$ cases three principal frequency response regions can be distinguished. As $\Omega \to 0$ all quantities approach limiting behavior. At some nonzero frequency an initial capacitative dispersion region appears, finally followed, when $\Omega \gg 1$, by limiting high-frequency behavior. Particularly in the first two regions, results for the two boundary condition situations are quite different. Principal results of the present and previous work[10] are summarized in Table I to allow convenient cross comparison of the three regions for the two cases of interest. All the results given in this table (except those applying for $\Omega \to 0$) are approximate, but in the intervals listed the approximations are excellent.

For simplicity, the expressions in Table I apply only for $M \gtrsim 3$. Results for $M < 3$ are readily derived from the expressions already given herein and in Ref. 10. Note that for $M \gg 1$, many of the quantities listed simplify considerably. For example, $s_b \to M$, $s_d \to M^2/12$, $\Lambda_b \to M^2$, $\Lambda_d \to 7M^4/180$, $\Lambda_b/s_b \to M$, $s_b^2/\Lambda_b \to 1$, and $4s_d^2/\Lambda_d \to 5/7$. For completeness, Table II lists approximate values of the quality factor $Q \equiv (\omega C_P/G_P) = (\omega C_S/G_S)^{-1}$. Note that the corresponding loss tangent, $\tan\delta$, is given by $Q^{-1} \equiv \omega C_S/G_S$. Comparison with Table I shows how Q enters the various approximate relations given there. The present Q goes to infinity as $\omega \to 0$ and toward zero as $\omega \to \infty$. Its dependence on Ω is monotonic for both boundary condition situations.

I have not listed C_{PN} and C_{SN} expressions in Table I since they may be readily obtained from the C_P/C_g and C_S/C_g results by dividing by the appropriate s. The initial values of C_{PN} and C_{SN} are unity. The values of Ω by which these quantities have decreased to 0.5 are of interest. For the $(0, 0)$ case, these values are s_b/Λ_b and $\gtrsim 7$, respectively, for any M. Alternatively, for the $(0, \infty)$ situation the values of Ω are approximately $4M^{-2}$ $(M \gtrsim 10^2)$ and $50M^{-2}$, respectively. It follows from Table I that for $M \gtrsim 10^2$, the Ω value at which the $(0, 0)$ and $(0, \infty)$ C_P's are equal is about $\Omega \equiv \Omega_P \cong (2M^4)^{-1/3}$. The important variable $M^2\Omega$ is thus about

TABLE I. Dependence of normalized capacitance and conductance on relative frequency, $\Omega \equiv \omega\tau_D$, for $M \gtrsim 3$.

	Parallel quantities					Series quantities				
	C_P/C_g			G_{PN}		C_S/C_g		G_{SN}		
Conditions	$(0, 0)$	$(0, \infty)$	s_d	$[G_P/G_\infty]$ $(0, 0)$	$[G_P/(G_\infty/2)]$ $(0, \infty)$	$(0, 0)$	$(0, \infty)$	s_d	$[G_S/G_\infty]$ $(0, 0)$	$[G_S/(G_\infty/2)]$ $(0, \infty)$
$\Omega \to 0$	s_b		s_d	$\Lambda_b\Omega^2$	$\Lambda_d\Omega^2$	s_b		s_d	s_b^2/Λ_b	$4s_d^2/\Lambda_d$
$(0, 0)$: $0 \leq \Omega \lesssim 1$ $(0, \infty)$: $(10/M)^2 \lesssim \Omega \lesssim 0.1$	$\dfrac{s_b}{1+(\Lambda_b\Omega/s_b)^2}$		$1/\Omega[2M^2\Omega]^{1/2}$	$\dfrac{\Lambda_b\Omega^2}{1+(\Lambda_b\Omega/s_b)^2}$	$1-(2/M^2\Omega)^{1/2}$	s_b		$[M^2/8\Omega]^{1/2}$	s_b^2/Λ_b	$\dfrac{1}{1+(M^2\Omega/2)^{-1/2}}$
$\Omega \gg 1$	$\dfrac{1}{\Omega[2M^2\Omega]^{1/2}}$		$1/\Omega[8M^2\Omega]^{1/2}$	$1-(1/2M^2\Omega)^{1/2}$	$1-(1/2M^2\Omega)^{1/2}$	$[2M^2/\Omega]^{1/2}$	$[M^2/2\Omega]^{1/2}$		$\dfrac{1}{1+(2M^2\Omega)^{-1/2}}$	$\dfrac{1}{1+(2M^2\Omega)^{-1/2}}$

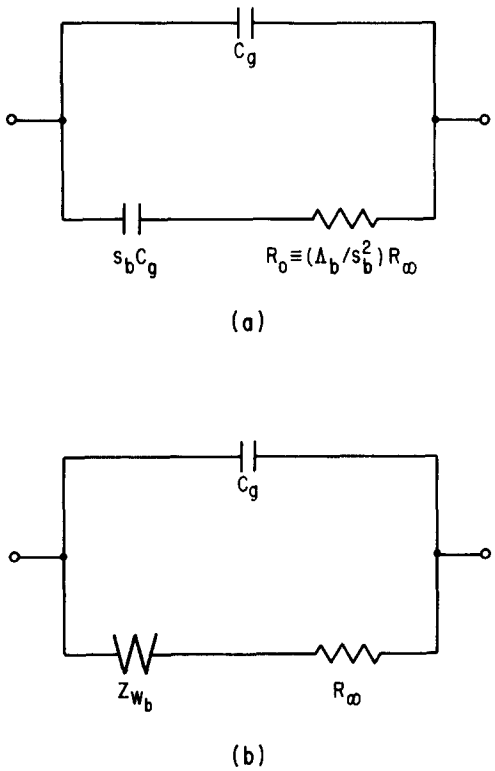

FIG. 5. Equivalent circuits for (0, 0) boundary conditions. Approximate domains of applicability: (a) $0 \leq \Omega \lesssim 1$; (b) $\Omega \gg 1$.

$(0.5M^2)^{1/3}$ at this point. One also finds that the Ω value at which the respective C_S values are equal is about 0.125. Thus, the actual value of C_S for the $(0, \infty)$ situation will exceed that for the (0, 0) case over most of the frequency range of ordinary interest $(0 \leq \Omega \lesssim 1)$. Note, however, that $(C_0 - C_g)$ for the $(0, \infty)$ case only exceeds that for (0, 0) when $M > (3/2)[3+(5)^{1/2}] \cong 7.85$.

V. (0, 0) SITUATION

A. Equivalent Circuits

In the (0, 0) ideal-polarized-electrode case, earlier work[1,10] led to an equivalent circuit made up of C_g in parallel with a single branch consisting of a series combination of a resistance R_S and capacitance C_S. The impedance of this series branch, Z_S, is $Y_P^{-1} = [Y_T - i\omega C_g]^{-1}$. For $0 \leq \Omega \lesssim 1$, R_S and C_S were found to be essentially frequency independent, leading to the equivalent circuit of Fig. 5(a). I have represented the space-charge part of the capacitance (the double-layer capacitance), $(C_0 - C_g)$, by s_bC_g to distinguish it from the different $(C_0 - C_g)$ which applies in the $(0, \infty)$ situation. Note that for large M, $s_bC_g \equiv (M-1)C_g \cong MC_g$, and the resistance shown, R_0, approaches $R_\infty \equiv G_\infty^{-1}$. The series branch yields simple Debye dispersion in this $0 \leq \Omega \lesssim 1$ normalized frequency range and is consistent with the corresponding results listed in Table I.

Table I shows that for (0, 0) and $\Omega \gg 1$, $R_S \equiv G_S^{-1} \cong [1+(2M^2\Omega)^{-1/2}]R_\infty$. Thus for $\Omega \to \infty$, $R_S \to R_\infty$, the bulk resistance of the material. R_S is within 1% of R_∞ at $\Omega = 5 \times 10^3/M^2$, a value less than unity for $M > 10^2/\sqrt{2}$. We may now define an interface impedance Z_i by removing the limiting resistance R_∞ from Z_S. Therefore, $Z_i \equiv Z_S - R_\infty \equiv R_{Si} + (i\omega C_S)^{-1}$, where $R_{Si} \equiv R_S - R_\infty$. For the region of applicability of Fig. 5(a), $R_{Si} \simeq R_\infty/2M$ for $M \gg 1$. Thus, it will frequently be negligible compared to R_∞.

One may derive Z_i itself directly for all Ω from the results of earlier work[10] by recognizing that the complex quantity N given there is $Y_T/i\omega C_g$. Direct calculation then gives, after simplification,

$$Y_{iN} \equiv \frac{Y_i}{G_\infty} \equiv Z_{iN}^{-1}$$

$$= \frac{i\Omega\{M(1+i\Omega)^{1/2} \coth[M(1+i\Omega)^{1/2}] - 1\}}{1+i\Omega}. \quad (9)$$

Later on this important result will be used further.

The results of Table I, or Eq. (9), lead for $\Omega \gg 1$ to

$$R_{Si} \cong (2M^2\Omega)^{1/2}R_\infty = [R_\infty/2M^2C_g\omega]^{1/2} = \eta_b/(\omega)^{1/2}, \quad (10)$$

and

$$C_S \cong [2M^2/\Omega]^{1/2}C_g$$
$$= [2M^2C_g/R_\infty\omega]^{1/2}$$
$$= \eta_b^{-1}/(\omega)^{1/2} \equiv C_{W_b}$$
$$= (\sqrt{2}l_d/L_D)(\epsilon/8\pi L_D), \quad (11)$$

where

$$\eta_b \equiv [R_\infty/2M^2C_g]^{1/2} = (kT/e^2c_0)(2D_n)^{-1/2}, \quad (12)$$

and we have used $\mu_n/D_n = e/kT$. Note that η_b is an intrinsic property of the material as it should be. For $M \gtrsim 3$, $C_0 \cong MC_g \cong \epsilon/8\pi L_D$, where C_0 is the total low-frequency-limiting capacitance/unit area. Substituting for M in Eq. (12), one obtains $\eta_b \cong C_0^{-1}[\tau_D/2]^{1/2}$.

The series combination of C_S and R_{Si}, the interface impedance Z_i, is equal in the present range to the Warburg impedance[11]

$$Z_W \equiv \eta(1-i)/(\omega)^{1/2}, \quad (13)$$

where here $\eta = \eta_b$ and $Z_W = Z_{W_b}$. The corresponding parallel components of Z_W^{-1} are $Y_W \equiv (\omega)^{1/2}(1+i)/2\eta$. Note that we may also write $(Z_{W_b}/R_\infty) = (iM^2\Omega)^{-1/2}$,

Table II. Approximate expressions for Q in various regions.

Conditions	(0, 0)	(0, ∞)
(0, 0): $0 \leq \Omega \lesssim 1$	$s_b/\Lambda_b\Omega$	$[2/M^2\Omega]^{1/2}$
(0, ∞): $(10/M)^2 \lesssim \Omega \lesssim 0.1$		
$\Omega \gg 1$	$[2M^2\Omega]^{-1/2}$	$[2M^2\Omega]^{-1/2}$

in agreement with Eq. (9) in this limit. Equations (10) and (11) for R_{Si} and C_S are in full agreement with standard Faradaic admittance results[12–14] applying when there is an infinitely fast reaction between a reacting electrode and a potential-determining univalent ion in a solution of indifferent electrolyte. Here, however, the Warburg impedance appears only for $\Omega \gg 1$, not for all Ω; there is no Faradic current; there are two electrodes; and no indifferent electrolyte is present. The present result demonstrates explicitly for the first time that the Warburg impedance appears (for $\Omega \gg 1$) with ideal polarized electrodes (no discharge, no reaction, no specific adsorption). This result is, of course, implicit in but was unrecognized in earlier work.[1,2,10] The reason for the appearance of Z_W is not far to find, however, and its presence not as surprising as it seems at first. For sufficiently high normalized frequencies ($\Omega \gg 1$), there is insufficient time for a space–charge layer to form in the neighborhood of a blocking electrode during a single half-cycle of the applied sinusoidal disturbance. There is then no ideal double layer capacitance, yet the current through the electrode is a pure displacement current and is controlled solely by plane diffusion.[15]

Figure 5(b) shows the equivalent circuit applicable for the (0, 0) situation when $\Omega \gg 1$. The conventional symbol for a Warburg impedance has been used here.[13] Now the ratio of C_0 to the series Warburg capacitance, C_{W_b}, of Eq. (11) is clearly $[\Omega/2]^{1/2}$, appreciably greater than unity for the $\Omega \gg 1$ region. Further, $C_{W_b}/C_g = M[2/\Omega]^{1/2}$ is itself also much greater than unity over a considerable part of the $\Omega \gg 1$ region when $M \gtrsim 10^2$, as it usually is in electrolyte situations. There is thus frequently a considerable span of Ω values over which C_{W_b} should be measurable. It is of interest to note that $\Omega C_{W_b}/C_g = [2M^2\Omega]^{1/2} = \tan\delta$, the loss tangent in this relative frequency range including R_∞, not that of the Warburg impedance alone, which is unity. More discussion of the implications of the present and succeeding results for the electrolyte double layer area will be presented in the final section.

B. Interface Quantities

In electrolyte double layer and reaction kinetics studies, much attention is given to the impedance of the interface double layer region, Z_i. Normalizing with R_∞, as in Eq. (9), leads one to $Z_{iN} = R_{SiN} + [i\Omega(C_s/C_g)]^{-1}$. Here, $R_{SiN} \equiv R_{Si}/R_\infty$. It is important to emphasize that over the entire range $0 \leq \Omega < \infty$, R_{Si} and C_S are independent of l for $M \gg 1$ and are hence thus truly intrinsic interface quantities in the present (0, 0) ideal polarized electrodes situation. For example, for $M \gg 1$ and $0 \leq \Omega \lesssim 1$, $C_S \rightarrow (C_0 - C_g) = s_b C_g \cong (M-1)C_g \cong MC_g = \epsilon/8\pi L_D$, and $R_{Si} \equiv R_S - R_\infty \rightarrow R_{Si0} \equiv R_0 - R_\infty \equiv [(\Lambda_b/s_b^2) - 1]R_\infty \cong [(M-2)/2(M-1)^2]R_\infty \simeq (2M)^{-1}R_\infty = L_D/(2\mu_n e c_0)$. In contradistinction it is clear from Table I that for $\Omega \gg 1$ the quantities C_P and $(G_\infty - G_P)$ are proportional to l^{-2} for $M \gg 1$. Further, for $M \gg 1$ and $(\Lambda_b\Omega/s_b)^2 \gg 1$, the results of Table I also show that $C_P \propto l^{-2}$ and $G_P \propto l^{-1}$.

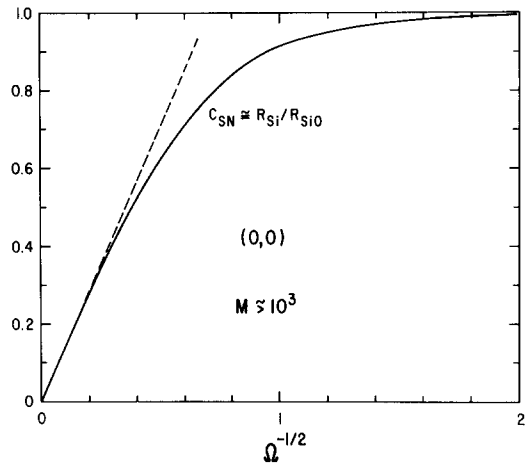

FIG. 6. The normalized interface quantities C_{SN} and R_{Si}/R_{Si0} vs $\Omega^{-1/2}$ for $M \gtrsim 10^3$.

Thus, $C_P \propto l^{-2}$ for all $\Omega \gg (s_b/\Lambda_b) \cong M^{-1}$. Since the parallel quantities are dependent on l over most or all of the frequency range, only the series ones are here appropriate as interface or double layer elements. The dependence of C_P and C_S on the concentration c_0 is also of interest. For $\Omega \rightarrow 0$ and $M \gg 1$, they both are proportional to $c_0^{1/2}$. Alternatively, for $M \gg 1$ and $\Omega \gg 1$, they are both proportional to c_0 itself.

Figure 6, using $\Omega^{-1/2}$ as abscissa, shows the limiting Warburg behavior at the left and the final low-frequency approach to unity of the normalized interface quantities C_{SN} and R_{Si}/R_{Si0}. For $M \gtrsim 10^3$, these variables are essentially identical for all Ω. We may emphasize the other end of the significant frequency spectrum by plotting these quantities times $\Omega^{1/2}$ vs $\Omega^{1/2}$, as in Fig. 7. The final $\Omega \rightarrow \infty$ limiting value of both variables is $\sqrt{2}$. Also shown in Fig. 7 is $\delta_i = \tan^{-1}(Q_i^{-1})$, the loss angle for Z_i, not Z_P. Here the interface quality factor Q_i is given by $(\omega R_{Si}C_S)^{-1} \equiv (\Omega R_{SiN} s_b C_{SN})^{-1}$.

C. Transient Response

The response of the interface region to a step function of voltage, $V_0 u_0(t)$, is of especial interest since some approximation to it is commonly measured in electrolyte potentiostatic experiments.[16] Here $u_0(t)$ is the Heaviside unit step function, and the voltage V_0 is, as usual, taken as much less than kT/e in magnitude to ensure linear system response. Let $I_i(t)$ be the current that flows when $V_0 u_0(t)$ is applied to the initially uncharged electrode-interface region; for a linear system this is also the discharge current when the system charged to V_0 is suddenly short circuited.

Linear system response theory[17–19] yields $I_i(t) \equiv V_0 \mathfrak{L}^{-1}[Y_i(p)/p]$, where $\mathfrak{L}^{-1}$ denotes the inverse Laplace transform, and p (not to be confused with a positive charge concentration) is the complex transform variable, whose imaginary part is ω. Using Eq. (9), we first form

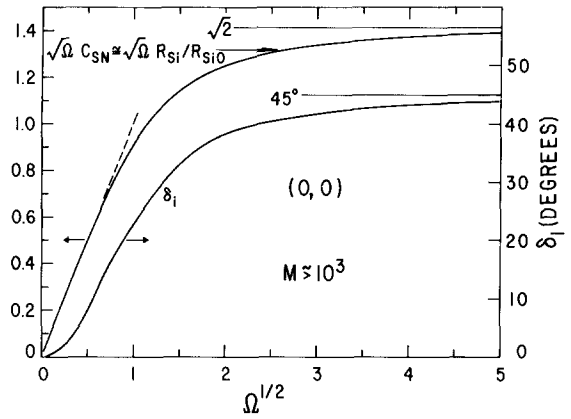

FIG. 7. The quantities $\Omega^{1/2}C_{SN}$, $\Omega^{1/2}R_{Si}/R_{SiO}$, and the interface loss angle $\delta_i=\tan^{-1}Q_i^{-1}$ vs $\Omega^{1/2}$ for $M\gtrsim 10^3$.

$Y_i/i\omega(C_0-C_g)\equiv Y_{iN}/i\Omega s_b$, then replace $i\Omega$ by $p\tau_D$ throughout. The result of the inverse transform is, in terms of the normalized current I_{iN},

$$I_{iN}\equiv\tau_D I_i/(C_0-C_g)V_0 = \frac{\exp(-t/\tau_D)}{(r-1)}\left\{\frac{M}{(\pi t/\tau_D)^{1/2}} \times\left[1+2\sum_{n=1}^{\infty}\exp\left(-\frac{n^2M^2}{t/\tau_D}\right)\right]-1\right\}. \quad (14)$$

We have plotted I_{iN} vs $(t/\tau_D)^{1/2}$ in Fig. 8 for several M values. For $t\lesssim 0.01\tau_D$, the $M=10^3$ curve is closely proportional to $t^{-1/2}$. There is no significant difference between the $M=10^3$ curves and those for larger M. Further, the only important difference between this curve and all those between $M=10$ and 10^3 arises only from the $M/(r-1)\cong M/(M-1)$ factor in (14), since the infinite series terms only become significant when $t/\tau_D\gtrsim M^2$, a region where I_i will have decayed to too small a value to measure for $M\gtrsim 10$. The dashed $M=10^3$ curve of Fig. 8 is plotted semilog, using the top abscissa scale, rather than log-log. We see that the actual response for $0.04\lesssim t/\tau_D<M^2$, which is proportional to $(t/\tau_D)^{-1/2}\exp(-t/\tau_D)$, would certainly be mistaken for pure exponential decay if somewhat inaccurate experimental data of limited time span were used and no attempt were made to fit to the form of (14). Further, one would be very tempted to identify the response as the sum of two exponentials since end filtering gives an initial curve which is essentially straight for $(t/\tau_D)^{1/2}\gtrsim 0.02$.

The superb approximation of omitting the infinite series terms for $M\gtrsim 10$ is equivalent to approximating the $M\gg 1$ frequency response by

$$Y_{iN}\cong i\Omega M/(1+i\Omega)^{1/2} \quad (15)$$

in place of (9). This simple and significant result will be discussed later.

Sometimes the charge, as well as or instead of current, is examined. Let

$$q_i(t)\equiv\int_0^t I_i(t)\,dt$$

and actually consider $q_{iN}\equiv q_i/(C_0-C_g)V_0$, the effective time-varying capacitance, normalized to unity at $t=\infty$. We find

$$q_{iN}=\frac{M}{r-1}\left(\operatorname{erf}\left(\frac{t}{\tau_D}\right)^{1/2}+\sum_{n=1}^{\infty}\left\{\exp(2nM)\times\operatorname{erf}\left[\left(\frac{t}{\tau_D}\right)^{1/2}+\left(\frac{nM}{(t/\tau_D)^{1/2}}\right)\right]+\exp(-2nM)\times\operatorname{erf}\left[\left(\frac{t}{\tau_D}\right)^{1/2}-\left(\frac{nM}{(t/\tau_D)^{1/2}}\right)\right]-2\sinh M\right\}\right) -(r-1)^{-1}\left[1-\exp\left(-\frac{t}{\tau_D}\right)\right]. \quad (16)$$

It is readily verified that as $t\to\infty$, $q_{iN}\to 1$. Figure 9 shows computer-calculated results for $M=1$, 3, and 10^3. Again, all series terms may be neglected for $M\gtrsim 10$. Clearly for $0\leq(t/\tau_D)^{1/2}\lesssim 0.3$, $q_i(t)$ is accurately proportional to $t^{1/2}$ for $M\gtrsim 10^3$.

It should be pointed out that when the transient response of the Z_S rather than the Z_i part of the system is considered, the current $I_P(t)$ which flows upon application of $V_0u_0(t)$ to the originally uncharged system has an initial value not of infinity, as in Fig. 8, but of V_0/R_∞. For comparison, the corresponding initial value of $I_{PN}\equiv\tau_D I_P/(C_0-C_g)V_0$ is M^{-1} for $M\gg 1$. Although it is pos-

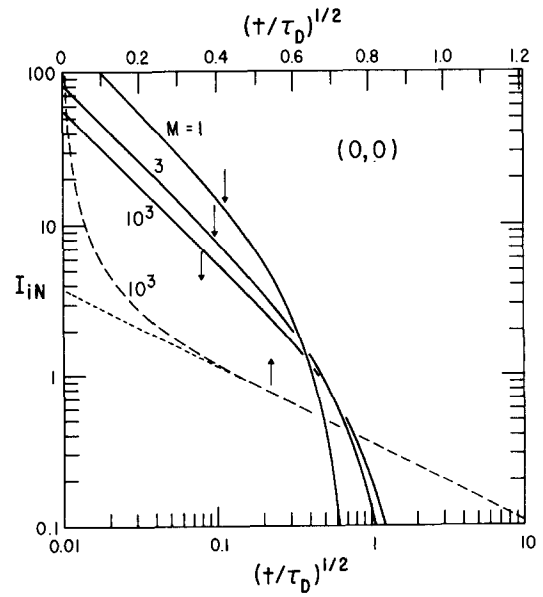

FIG. 8. The normalized interface charging current I_{iN} in response to a step function of applied potential vs $(t/\tau_D)^{1/2}$ for several M values; log-log and semilog representations.

sible to carry out the inverse Laplace transform of $Y_{PN}(p)/p$ when $M \gg 1$ so that (15) is applicable, the result is still quite complicated and will not be given here. The final value theorem of transform theory shows in this case that, as expected, $q_P(t)$ still approaches, as it must, $(C_0 - C_g)V_0 = s_b C_g V_0$ as $t \to \infty$. The time required to achieve essentially this final value will generally be much longer than τ_D, of course, and is of the order of $M\tau_D$ for $M \gg 1$.

VI. (0, ∞) SITUATION

A. Equivalent Circuits

In this case, the results already given allow us to construct the three equivalent circuits of Fig. 10. In Fig. 10(a) note that for $M \gg 1$, $s_d C_g \cong M^2 C_g/12$, and $R_0 \cong (14/5)R_\infty$. Further, the two separate $2R_\infty$ resistances which appear in Figs. 10(b) and 10(c) are only equal because of our present simplifying choice $\mu_n = \mu_p$. The parallel $2R_\infty$ branch here arises from the discharging negative charge carriers; the other $2R_\infty$ resistance must therefore be associated with the blocked positive carriers. The Warburg impedances in 10(b) and 10(c) are defined in the next section. In the limit of high frequencies, $\Omega \to \infty$, $Z_W \to 0$, and the parallel combination of the two resistive branches is just $R_\infty^{-1} = G_\infty \equiv ec_0(\mu_n + \mu_p)/l = 2\mu_n e c_0/l$ as it must be. Note, however, that R_S is only within 1% of $2R_\infty$ for $M^2\Omega > 5 \times 10^3$.

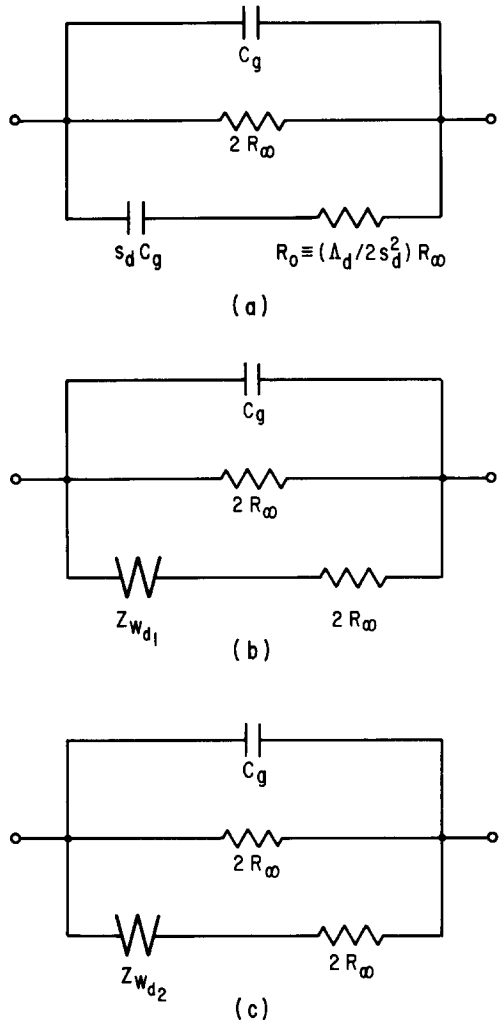

FIG. 10. Equivalent circuits for (0, ∞) boundary conditions. Approximate domains of applicability: (a) $0 \leq \Omega \lesssim 10/M^2$; (b) $(10/M)^2 \lesssim \Omega \lesssim 0.1$; (c) $\Omega \gg 1$.

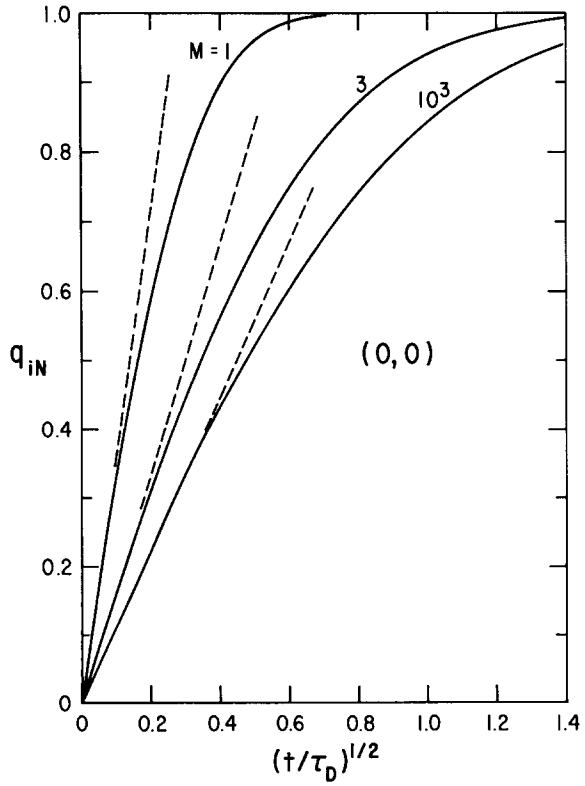

FIG. 9. The normalized interface region charge q_{iN} vs $(t/\tau_D)^{1/2}$ for several M values.

Although Friauf[2] considers the $\mu_n \neq \mu_p$ case, he gives no exact closed-form expression for admittance or impedance and doesn't attempt to isolate a frequency-independent parallel conductance path. We can use Friauf's results, however, to provide $\mu_n \neq \mu_p$ generalizations to the (0, ∞) case C_P/C_g and G_P/G_∞ expressions of Table I for $(10/M)^2 \lesssim \Omega \lesssim 0.1$. If we write as before $\Omega \equiv \omega\tau_D$, with $\tau_D = C_g/G_\infty$, we must now use $G_\infty = ec_0(\mu_n + \mu_p)/l$; the expression for M already given remains unchanged. Friauf's results then lead to $C_P/C_g \cong \Omega^{-3/2}(2M^2)^{-1/2}N$ and $1 - (G_P/G_\infty) = \Omega^{-1/2}(2M^2)^{-1/2}N$, where the correction factor is

$$N \equiv [4D_n^3/D_p(D_n + D_p)^2]^{1/2}, \qquad (17)$$

equal to unity for equal diffusion coefficients. Here where negative charge carriers discharge, clearly N may

be much larger than unity if $D_n \gg D_p$. Then $N \simeq 2(D_n/D_p)^{1/2}$. Somewhat more surprising is the result that in this normalized frequency range when $D_n \to 0$, $C_P \to 0$ and $G_P \to G_\infty$. Note, however, that in the limit $D_n \to 0$ there will be no discharge. Here, of course, G_P involves all parallel conductance since no parallel branch containing part of G_∞ has been removed.

When $\mu_n \neq \mu_p$ and when there may be in addition some discharge of charge carriers of both signs, it still seems possible and important to remove a frequency-independent parallel conductance branch from Y_T as in the present work. Such a branch will provide the needed direct path for the discharge current which flows. Its value, which may involve both μ_n and μ_p, must equal the $\Omega \to 0$ value of $\mathrm{Re}(Y_T)$. Although the analysis has not yet been carried out in the general case, I believe removal of such a branch is essential, as it is in the present $(0, \infty)$, $\mu_n = \mu_p$ situation, to the establishment of the most meaningful and useful equivalent circuit for the over-all system.

B. Interface Quantities

An "interface" impedance, $Z_i \equiv R_{Si} + (i\omega C_S)^{-1}$, may be defined in the present $(0, \infty)$ case by the same procedure used in the blocking situation. First, note that $Z_S \equiv Y_P^{-1} = \{Y_T - [i\omega C_g + (l/\mu_n e c_0)]\}^{-1}$. Since here $R_S \to 2R_\infty = l/\mu_p e c_0$ as $\Omega \to \infty$, it is evident that Z_i should be defined as $Z_S - (l/\mu_p e c_0)$, rather than the $Z_S - R_\infty$ of the $(0, 0)$ case. I have distinguished above between the two $2R_\infty$ terms, $l/\mu_n e c_0$ and $l/\mu_p e c_0$, in order to indicate how the subtractions should be made in an unequal mobility case. Normalized quantities of interest are $Z_{iN} \equiv Z_i/2R_\infty$ and $R_{SiN} \equiv R_S/2R_\infty$. Now the prescription given above for Z_i yields

$$Y_{iN} \equiv Y_i/(\tfrac{1}{2}G_\infty) \equiv Z_{iN}^{-1}$$
$$= [i\Omega/2(1+i\Omega)](M(i+i\Omega)^{1/2} \coth[M(1+i\Omega)^{1/2}]$$
$$-2+(i\Omega)^{-1}\{M(i\Omega)^{1/2}(1+i\Omega) \coth[M(i\Omega)^{1/2}]-1\}). \quad (18)$$

Since there are two successive $C_s \propto \Omega^{-1/2}$ regions in the present discharge situation, we may expect to find two separate Warburg impedances, applying for different frequency regions. In the blocking situation, the Warburg impedance was associated with a series R_∞. Here, however, Z_W is associated with $2R_\infty$. The results of Table I lead to

$$Z_i \to Z_{Wd_1} \equiv \eta_{d_1}(1-i)/(\omega)^{1/2}$$

for $(10/M)^2 \lesssim \Omega \lesssim 0.1$ and to

$$Z_{Wd_2} \equiv \eta_{d_2}(1-i)/(\omega)^{1/2}$$

for $\Omega \gg 1$. Here

$$\eta_{d_1} \equiv [8R_\infty/M^2 C_g]^{1/2} = (kT/e^2 c_0)(D_n/8)^{-1/2} \quad (19)$$

and

$$\eta_{d_2} \equiv [2R_\infty/M^2 C_g]^{1/2} = (kT/e^2 c_0)(D_n/2)^{-1/2}. \quad (20)$$

Since η_{d_1} and η_{d_2} are independent of l, C_S and R_{Si} are properly intrinsic interface quantities in the region $(10/M)^2 \lesssim \Omega \leq \infty$.

Alternatively, the present results may be expressed as

$$(Z_{W_{d_1}}/2R_\infty) = 2/(iM^2\Omega)^{1/2}$$

and

$$(Z_{W_{d_2}}/2R_\infty) = (iM^2\Omega)^{-1/2},$$

equal to (Z_{W_b}/R_∞). The equality of the $\Omega \gg 1$ normalized Warburg impedances for the $(0, 0)$ and $(0, \infty)$ situations is a necessary result. The high-frequency limit for the impedance arising from mobile charges must be essentially the same in the two cases. The factor of 2 difference in the actual impedance magnitudes and hence between η_{d_2} and η_b arises from the presence of equally mobile charges of both signs in the $(0, 0)$ case, while only positive charges effectively contribute to the series $2R_\infty$ and the Warburg impedance in the present $(0, \infty)$ case. More interesting is the ratio

$$Z_{W_{d_1}}/Z_{W_{d_2}} = \eta_{d_1}/\eta_{d_2} = 2$$

found here. No obvious simple physical explanation presents itself for η_{d_1}, applying at lower relative frequencies, to be twice η_{d_2}. On the other hand, $Z_{W_{d_1}}/2$, the impedance associated with only one of the two electrodes, agrees with the usual single-electrode Warburg result for a redox reaction involving univalent ions having equal diffusion coefficients and equal bulk concentrations.

Let us next consider the low-frequency region of

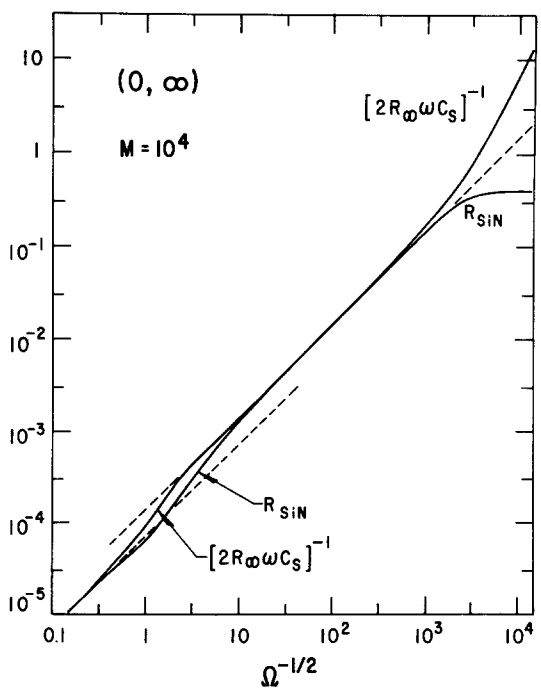

FIG. 11. Log–log plot showing dependence of the reactive and resistive components of Z_{iN} on $\Omega^{-1/2}$ for $M = 10^4$.

approximate constancy of Z_S and Z_i: $0 \leq \Omega \lesssim (10/M^2)$. Now as $\Omega \to 0$, $C_S \to (C_0 - C_g) = s_d C_g$. Equation (5) yields $C_S \to (M^2/6)C_g$ as $M \to 0$. For the more interesting case of $M \gtrsim 3$, we find $(C_0 - C_g) \cong \{(M^2/12) + [(M-1)/4]\} C_g$. The first term will be much larger than the others for almost all cases of practical interest ($M \gg 1$). This term is proportional to l and to c_0; the second term is independent of l; and the final term is inversely proportional to l. Using Eq. (8), we also find for $M \gg 1$,

$$R_{SiN} \underset{\Omega \to 0}{\to} [(1-G_{0N})/(G_{0N}]$$

$$\cong (\tfrac{1}{90}M^4 + \tfrac{1}{2}M - \tfrac{1}{2})/(\tfrac{1}{36}M^4 + \tfrac{1}{6}M^3 + \tfrac{1}{12}M^2 - \tfrac{1}{2}M + \tfrac{1}{4})$$

$$\simeq \tfrac{2}{5}, \qquad (21)$$

where the final ratio applies for $M \to \infty$. Therefore, for large M and $\Omega \to 0$, $R_{Si} \to R_{Si0} \simeq 4R_\infty/5$ and is also proportional to l, unlike the $(0, 0)$ R_{Si} which is independent of l.

In the range $\Omega \lesssim (10/M^2)$, which varies as l^{-2}, we thus find the dominant terms of C_S and R_{Si} both proportional to l and hence extensive, not intensive quantities! The larger the l, the larger the low-frequency limiting capacitance but the smaller the frequency range over which it is applicable. For example, if $\Omega = 1$ corresponds to $\omega = 10^7$ rad/sec and if $M = 10^4$, this frequency range extends up to only about $\omega = 1$ rad/sec. Note that in this case, however, $(C_0 - C_g)$ is $M/12 \cong 833$ times larger in the $(0, \infty)$ case than in the blocking $(0, 0)$ case! Predominant discharge of a charge carrier of a single sign with $M \gg 1$ may be a partial explanation for the exceptionally large value of $C_0 \sim 15\ \mu F/\text{cm}^2$ found by Solomon, Sher, and Muller[20] for a small single crystal sample of LaF_3. The explanation can only be partial, however, because these authors found C_0, determined from integration of the current discharge in a transient response experiment, to be proportional to V_0, the charging voltage applied, rather than independent of V_0.

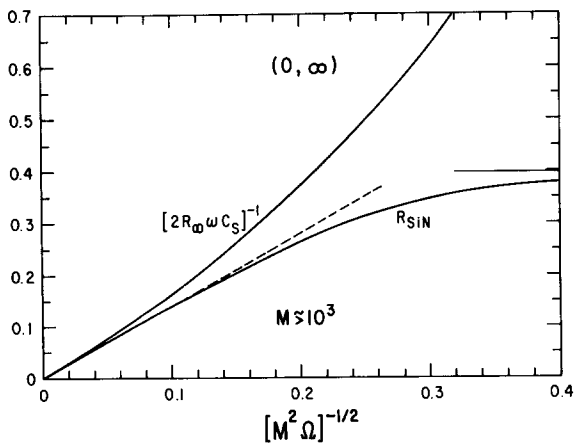

FIG. 12. Linear plot showing how $[2R_\infty \omega C_S]^{-1}$ and R_{SiN} depend on $(M^2\Omega)^{-1/2}$ for $M \gtrsim 10^3$.

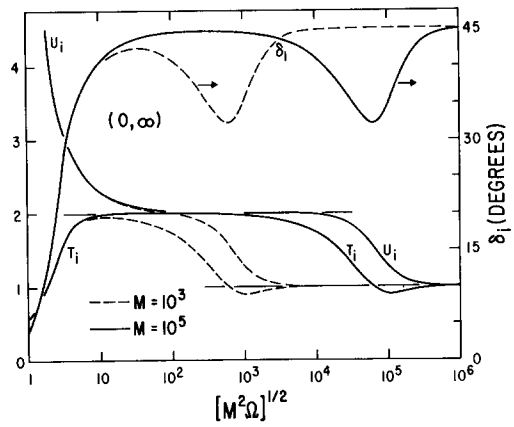

FIG. 13. Dependence of the resistive and reactive quantities T_i and U_i on $(M^2\Omega)^{1/2}$ showing Warburg regions for $M = 10^3$ and 10^5. Also shown is the loss angle δ_i.

The surprising proportionality to l of what should be intrinsic interface quantities is the reason we put the word "interface" in quotations when it first appeared in this section. Clearly, for $\Omega \lesssim (10/M^2)$ the prescription followed to obtain Z_i does not yield an intrinsic impedance. To obtain one, we must, for large M, subtract R_S and subtract $\{(M^2/12) - (1/4)\} C_g$ from C_S. The remaining true interface impedance in the present case is made up only of the space-charge capacitance $MC_g/4$. The dominant capacitance, $(M^2/12)C_g$, clearly does not arise from interface space charge. More light will be shed on this matter later.

Figure 11 shows how the components of Z_{iN}: the normalized "interface" reactance, $(\omega C_S)^{-1}/2R_\infty \equiv (2s_d \Omega C_S)^{-1}$, and resistance, R_{SiN}, depend on $\Omega^{-1/2}$. Note the transition from the final $\Omega \to \infty$ Warburg behavior at the left to the lower-frequency Warburg response, which finally gives way at sufficiently low relative frequencies to a constant R_{SiN} and a capacitative reactance proportional to Ω^{-1}. The lower-frequency response is plotted on a linear scale in Fig. 12 using $(M^2\Omega)^{-1/2}$ as abscissa in order to make the results closely applicable for all $M > 100$ or so.

Deviations from Warburg behavior show up quite well if we define and examine $T_i \equiv (2M^2\Omega)^{1/2} R_{SiN}$ and $U_i \equiv (2M^2\Omega)^{1/2}(2s_d \Omega C_S)^{-1}$, where we have divided the quantities of Figs. 11 and 12 by their final $\Omega \to \infty$ mutual Warburg response value. Figure 13 shows how these quantities, and the loss angle δ_i, depend on $(M^2\Omega)^{1/2}$ for $M = 10^3$ and 10^5. The two Warburg regions, with ordinates 2 and 1, stand out clearly.

The "interface" admittance Y_i may be written $Y_i \equiv G_{iP} + i\omega C_{iP}$, where the P subscript is used to indicate parallel connection. Sometimes the real and imaginary parts of Z_S, Z_i, Y_P, or Y_i have been plotted against each other in the complex plane, as in the circle diagram of electrical engineering. De Levie[15] has proposed plotting

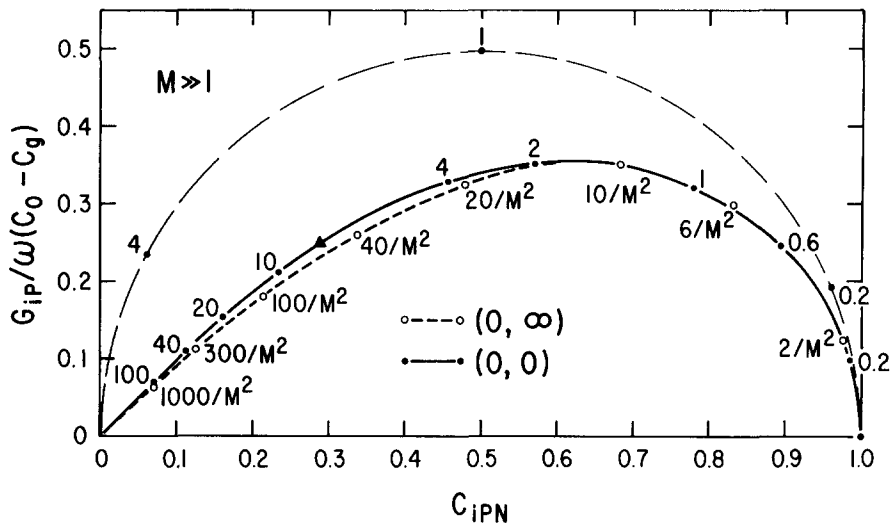

FIG. 14. Cole–Cole plot of components of $Y_i/i\omega(C_0-C_g)]$. The figures on the curves are values of $\Omega\equiv\omega\tau_D$. The semicircle shows the behavior of simple Debye dispersion.

the parts of Y_i/ω in this fashion and shown it to be a useful approach. I believe a slightly better procedure, consistent with hallowed usage in dielectric response analysis, is to consider instead $Y_i/i\omega=C_{iP}-i(G_{iP}/\omega)$. Since $C_{iP}\rightarrow(C_0-C_g)$ as $\Omega\rightarrow 0$, it is finally desirable to use the normalized quantity $Y_i/[i\omega(C_0-C_g)]=Y_{iN}/2i\Omega s_d$ ($Y_{iN}/i\Omega s_b$ for the blocking case), plotting the real part on the real axis and the magnitude of the imaginary part on the imaginary axis. With the present normalization, this is completely equivalent to plotting the real and imaginary parts of the usual dielectric function $(\epsilon^*-\epsilon_\infty)/(\epsilon_0-\epsilon_\infty)$, where ϵ^* is a complex dielectric constant whose real part reaches ϵ_0 as $\omega\rightarrow 0$ and falls to ϵ_∞ as $\omega\rightarrow\infty$. Such a construction, a parametric function of ω or Ω, is frequently termed a Cole–Cole plot.[21]

Figure 14 shows such a plot for both the (0, 0) and (0, ∞) situations with $C_{iPN}\equiv C_{iP}/(C_0-C_g)$. The points on the curves indicate values of Ω. The top semicircle is the result obtained for simple Debye dispersion, $(1+i\Omega)^{-1}$. Now Eq. (15) shows that for $M\gtrsim 10$, $Y_i/[i\omega(C_0-C_g)]\cong[M/(M-1)][1+i\Omega]^{-1/2}$ for the (0, 0) case. Except for the factor $M/(M-1)$, this is just the expression for Davidson–Cole dispersion[22] when the Davidson–Cole parameter β is 0.5. Such dispersion may be interpreted as arising from a continuous distribution of relaxation times. Glarum[23] has shown that it may arise from a diffusion situation; the present results identify it with another diffusion process, plane diffusion of charge carriers.

The (0, 0) curve of Fig. 14 was drawn for $M=1000$, where the difference between $M/(M-1)$ and unity can be neglected. The same curve, multiplied by $M/(M-1)$ is, however, also applicable for M values down to 10 or so. Very nearly the same shape is still found even for $M=1$, but the relative frequencies are then shifted clockwise in a nonlinear fashion.

Figure 14 indicates that the (0, ∞) curve is quite close to that for the (0, 0) situation, although the relative frequency magnitudes are quite different. The final $\Omega\rightarrow\infty$ Warburg region doesn't show up on the (0, ∞) curve for $M\gg 1$ since it then occurs too near the origin to be distinguished. Of course, the left, asymptotically linear, portion of both curves is nevertheless associated with Warburg response: that for $\Omega\rightarrow\infty$ in the (0, 0) case, and that associated with $\Omega\gtrsim 100/M^2$ for the (0, ∞) situation. Although the (0, ∞) curve is stated to hold only for $M\gg 1$, computer calculation shows a difference of less than 3% between $M=1$ and $M\gtrsim 10^3$ points evaluated at the same $M^2\Omega$ value such as 1, 10, or 100. Thus for practical purposes this curve holds for all M values of interest.

Although the shapes of the (0, 0) and (0, ∞) curves are similar, the difference in normalized frequency response precludes direct identification of the (0, ∞) results with Davidson–Cole dispersion even though the response may certainly be associated with a distribution of relaxation times if desired.[17]

C. Transient Response

Using Eq. (21) and the procedure already described for the (0, 0) case, we may readily calculate the current $I_i(t)$ for a step function of voltage applied to the part of the system described by Y_{iN} alone. We shall do so, using

$$Y_i/i\omega(C_0-C_g)\rightarrow Y_i(p)/p(C_0-C_g)\equiv Y_{iN}(p)/2p\tau_D s_d,$$

to allow comparison with the (0, 0) calculations, but must caution that the results are unlikely to correspond very well with potentiostatic measurements because of the l dependence of Z_i and Y_i. In fact, the present results show that potentiostatic methods are inappropriate in the (0, ∞) case for long times. Here it would be better to begin with Y_P instead of Y_i (that is, include the series $2R_\infty$ resistance in the system) and compare with experimental results obtained with the voltage step method,[16] where the step voltage is applied across

the entire system. To do so, one would need to subtract from the total system current that arising from the immediate charging of C_g and that flowing through the parallel discharge path. Unfortunately, the inverse transform associated with $Y_P/i\omega$ does not seem very tractable.

For the "interface" part of the system, we obtain

$$I_{iN}\equiv\frac{\tau_D I_i}{(C_0-C_g)V_0}$$
$$=\left(\frac{1+\exp(-t/\tau_D)}{4s_d}\right)$$
$$\times\left\{\left(\frac{\pi t}{M^2\tau_D}\right)^{-1/2}\left[1+2\sum_{n=1}^{\infty}\exp\left(-\frac{n^2}{(t/M^2\tau_D)}\right)\right]-1\right\}. \quad (22)$$

The great similarity to the (0, 0) result of Eq. (14) will be obvious. Here, however, the part which appeared in the (0, 0) expression is multiplied by the factor $(r-1)/4s_d$ which is much less than unity for $M\gg1$. The charge

$$q_i(t)\equiv\int_0^t I_i(t)\,dt$$

will thus largely arise from the part of the integrand not multiplied by $\exp(-t/\tau_D)$ and will not approach unity until $t/\tau_D\sim M^2$. Thus, unlike the (0, 0) situation the infinite series is important in the (0, ∞) case for all M. Rather than give an explicit expression for q_{iN} as before, we shall here content ourselves with showing computer calculated curves of this quantity.

Figure 15 shows the (0, ∞) "interface" region current dependence for several M values. Here we have actually plotted M^2I_{iN} rather than I_{iN} in order to bring curves for all M values as close together as possible. Further, we have used the time variable $(t/M^2\tau_D)^{1/2}$ rather than the $(t/\tau_D)^{1/2}$ employed in Fig. 8. The curves show that I_i exhibits $t^{-1/2}$ behavior for $(t/M^2\tau_D)^{1/2}\lesssim0.02$ and begins to fall off very rapidly for $(t/M^2\tau_D)^{1/2}\gtrsim0.6$. Calculations for different M values show that curves for all $M>10^3$ are virtually indistinguishable from the 10^3 curve. Even the $M=100$ curve falls very close to the $M=10^3$ curve. As M decreases from 10 towards unity, the curves again approach closer to the $M=10^3$ curve, as shown by that for $M=3$. The actual (0, ∞) $M=1$ curve is virtually undistinguishable from the $M=1$ curve for the (0, 0) case of Fig. 8. This isn't too surprising since they both involve essentially only the final Warburg region. Note that the semilog plot for $M=10^3$ shows no appreciable straight-line region of approximately exponential decay as it did in the (0, 0) case.

It is worth noting that in the (0, 0) case the initial $(t/\tau_D\ll1)$ current I_i (not the normalized current) is $MV_0/R_\infty(\pi t/\tau_D)^{1/2}$. In the main range of (0, ∞) $t^{-1/2}$ decay, $1\ll t/\tau_D\ll M^2$, I_i turns out to be one-fourth of

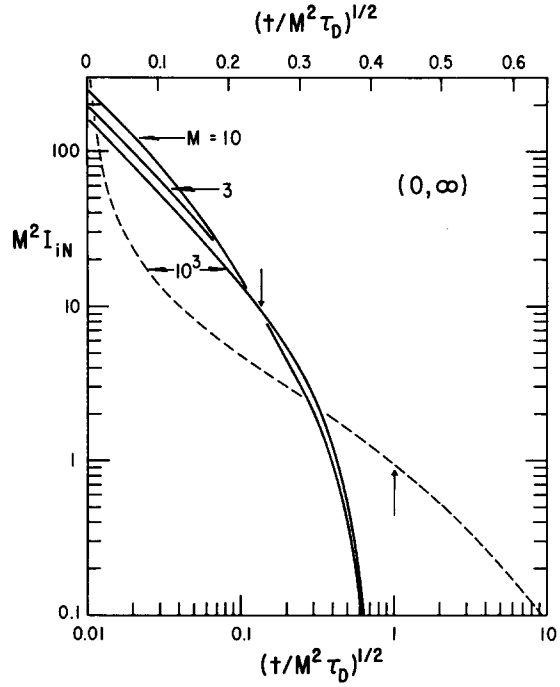

FIG. 15. The normalized charging current I_{iN} times M^2 vs $(t/M^2\tau_D)^{1/2}$ for several M values; log-log and semilog representations.

the above value. Thus, I_i is independent of l for both situations in these time intervals.

Figure 16 shows two calculated $q_{iN}\equiv q_i/(C_0-C_g)V_0$ curves. The shape of the $M=10^3$ curve is quite close to that of the (0, 0) $M=1$ curve of Fig. 9. There is still a region for $(t/M^2\tau_D)^{1/2}\lesssim0.05$, where $q_i(t)$ is proportional to $t^{1/2}$. Since M^2 may be very large indeed in practical situations, the region of $t^{\pm1/2}$ behavior for I_i and q_i can extend over a long, experimentally accessible time for the (0, ∞) case. Experimentally, t^{-n} current behavior with $n\sim0.5$ has been found[19] for a wide range of materials and conditions, from semi-insulating crystals to electrolytes.[23a]

Although the current decay we have discussed for the (0, 0) and (0, ∞) situations is never pure exponential and so precludes description in terms of a single time constant, we have seen that the times τ_D, $M\tau_D$, and $M^2\tau_D$ have entered naturally for $M\gg1$. Crudely speaking, τ_D is the time for step potentiostatic charging in the (0, 0) case; $M\tau_D$ that for voltage step charging in this case; and $M^2\tau_D$ the order-of-magnitude time for charging in the (0, ∞) case. In this latter case, charging of the Y_i region occurs by roughly $0.4M^2\tau_D$. For more experimentally accessible voltage step charging (step voltage applied across Y_P), the time for final charging should be roughly several times $2R_\infty(C_0-C_g)$, itself equal for $M\gg1$ to $(M^2/6)\tau_D$, again of order of magnitude $M^2\tau_D$.

It is of interest to examine how the three basic times above depend explicitly on ϵ, l, T, μ, and c_0, where μ is used to denote either μ_n or μ_p here. One readily finds: $\tau_D\propto\epsilon/\mu c_0$; $M\tau_D\propto(l/\mu)(\epsilon/c_0T)^{1/2}$; and $M^2\tau_D\propto l^2/\mu T$.

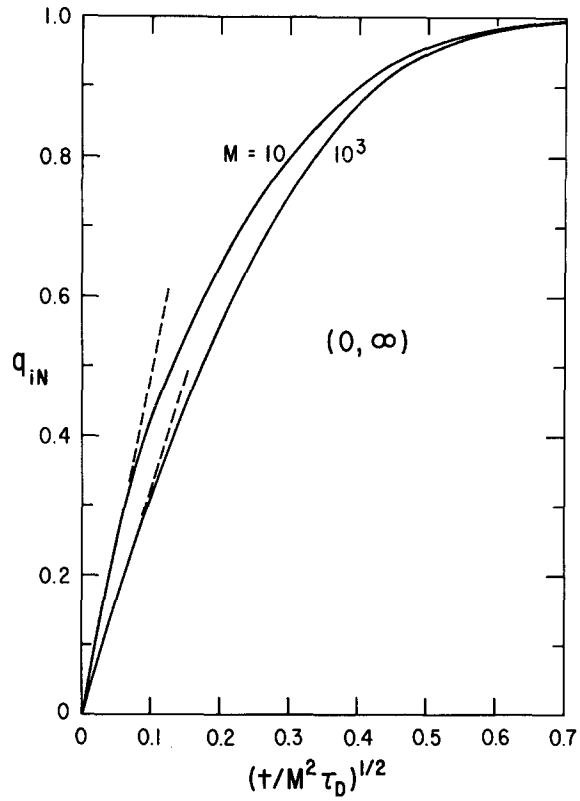

FIG. 16. The normalized charge q_{iN} vs $(t/M^2\tau_D)^{1/2}$ for $M=10$ and 10^3.

Note that while all depend on μ^{-1}, $M^2\tau_D$ is completely independent of concentration and dielectric constant. Since none of these times depends on applied voltage, no ordinary transit time is involved.

D. Space-Charge and Diffusion Capacitance

We have found that for $M\gg1$, $(C_0-C_g)\rightarrow MC_g\propto(\epsilon c_0/T)^{1/2}$ in the (0, 0) case, but $(C_0-C_g)\rightarrow M^2C_g/12\propto lc_0/T$ in the discharge situation. For the latter case, (C_0-C_g) may be increased indefinitely by increasing l, very different behavior from that of an ordinary plane-parallel capacitor such as C_g. Such behavior, is, however, reminiscent of that of the capacitance variation of two concentric spheres, having very different radii, as the larger radius increases. The present dependence of Z_i on l suggests that the usual failure to consider l as significant in an experimental electrolyte situation with discharge may explain some of the variability between the results of different investigators who thought they were isolating and comparing interface quantities alone.

The limiting capacitance (C_0-C_g) can reach tremendous values under ordinary conditions. For example, if $C_g=100$ pF and $M=10^5$, $(C_0-C_g)\cong(M^2/12)C_g=(1/12)$ F. Such large values are infrequently seen since they generally appear only at ultra-low frequencies. Nevertheless, all commercial solid capacitors show both some leakage (discharge or charge carriers of one or both signs) and the phenomenon of charge soakage. When charged over very long times they store much more charge than can be accounted for by their nominal (geometrical) capacitance. Motion of ions and/or electrons, holes, or charged vacancies associated with the present $(0, \infty)$ sort of mechanism is probably sufficient to explain this behavior. It is probably also the explanation of the tremendous 0.1 C of charge collected in the several-week discharge of a small F-centered KBr single crystal capacitor with $C_g\lesssim1$ pF and $R_\infty\sim10^7$ Ω.[24] Charging currents for these units also frequently showed a $t^{-1/2}$ behavior extending over long times. If the present $(0, \infty)$ treatment were directly applicable (unlikely, since one would not expect equal mobilities and completely free discharge of charge carriers of one sign), the above room-temperature results could be at least partially explained with $M\sim10^5$, $L_D\sim10^{-5}$ cm, $c_0\sim3\times10^{14}$ cm^{-3}, and a mobility of about 10^{-3} cm^2/V·sec. Since $\tau_D\sim10^{-5}$ sec, the corresponding approximate time constant for final charge or discharge, $M^2\tau_D$, is about 10^5 sec$\cong$28 h.

The very large possible values of (C_0-C_g) and its dominant extrinsic character make one wonder about the space-charge distribution in the material. How much of the low-frequency capacitance is associated with the space charge? For simplicity, we shall examine the space-charge distribution for $\Omega\rightarrow0$. Let $V_1^*\equiv eV_1/kT$, where V_1 is, as usual, the amplitude of the applied sinusoidal voltage. Then define $n_1^*\equiv n_1/c_0V_1^*$, $p_1^*\equiv p_1/c_0V_1^*$, and $W\equiv(2x/l)-1$. Here p_1 is the amplitude of the sinusoidal component of positive charge concentration. Table III summarizes the results obtained for these normalized charge amplitudes for $\Omega\rightarrow0$ and a positive voltage applied to the electrode at $x=0$.

Figure 17 shows the dependence on position of these charges for $M=10$. This small a value of M has been used to expand for clarity the curved portions of the graph, which appear only very near $W=\pm1$ for larger M values. In both the table and figure we have actually considered results for the $(\infty, 0)$ situation rather than the $(0, \infty)$ one. The total positive charge is given in the present linearized case by the real part of $p=c_0+p_1\exp(i\omega t)$, with a similar expression for n. Figure 17 shows that p always remains equal to c_0 at the boundaries, as required by the $(\infty, 0)$ boundary condition of

TABLE III. Comparison of normalized charge amplitudes for the (0, 0) and $(\infty, 0)$ situations at $\Omega=0$ as functions of $W\equiv(2x/l)-1$.

	n_1^*	p_1^*
(0, 0)	$-(\sinh MW\ \mathrm{csch}M)/2$	$(\sinh MW\ \mathrm{csch}M)/2$
$(\infty, 0)$	$-\dfrac{(\sinh MW+W\sinh M)}{4\sinh M}$	$\dfrac{(\sinh MW-W\sinh M)}{4\sinh M}$

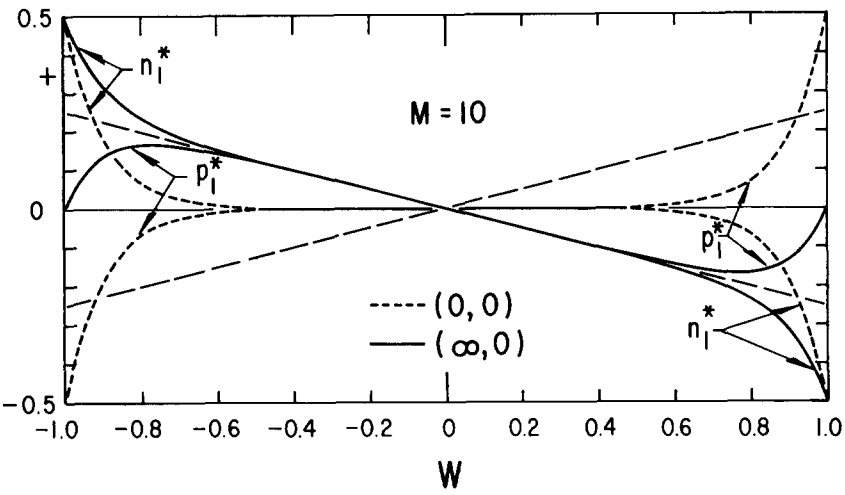

FIG. 17. Dependence of the sinusoidal components of the normalized charge concentrations on $W \equiv (2x/l) - 1$ for $M = 10$, $(0, 0)$ and $(\infty, 0)$ cases.

free discharge of positive carriers. Further, since the maximum value of the normalized quantities is 0.5, the maximum perturbation of the original concentration c_0 is $\pm V_1^* c_0/2$. Since V_1^* is, by the linearizing hypothesis, much smaller than unity, the perturbation is much less than c_0, as it must be since negative concentrations are unphysical.

The table and figure show that in the $(0, 0)$ case there is indeed an interface region at each electrode and an unperturbed bulk region. For the $(0, \infty)$ situation, however, the charge distributions are everywhere perturbed because of the discharge current (except at $W = \pm 1$ for p_1^*). It is very significant, nevertheless, that the space-charge density, $\rho_1 \equiv e(p_1 - n_1)$, is only appreciably different from zero near the electrodes for both cases. (This behavior also holds as well for $\Omega > 0$.) In fact, for $\Omega \to 0$ the $\rho_1 = (ec_0 V_1^*)(\sinh MW \operatorname{csch} M)/2$ for $(0, \infty)$ is just half of the ρ_1 applicable for $(0, 0)$, even though $(C_0 - C_g)$, as calculated from the ac response with $\Omega \to 0$, is extrinsic and generally far larger for $(0, \infty)$ than for $(0, 0)$.

If we integrate ρ_1 from $W = 0$ to $W = 1$ and divide by V_1, we obtain a static space-charge capacitance C_{SC0}, equal to $(MC_g/2)(\operatorname{ctnh} M - \operatorname{csch} M)$ in the discharge case. This capacitance should not include C_g directly and should therefore go to zero as $M \to 0$. We see that it is nowhere near the ac $(C_0 - C_g) \cong (M^2 C_g/12)$ appropriate for $M \gg 1$ in the $(0, \infty)$ case. For the blocking situation, C_{SC0} is twice the above value and does approach $(C_0 - C_g) = (r-1)C_g \cong MC_g$ for $M \gg 1$. These results again make it evident that the large $(0, \infty)$ $(C_0 - C_g)$ is not primarily associated with the space charge localized near a given electrode. Such space charge *is* intrinsic and interfacial for $M \gg 1$ just as in the $(0, 0)$ case. Thus, an interface or interphase region abutting an electrode can be isolated even in the present case if it is defined as the region where electroneutrality fails, but its capacitance and resistance must *not* be identified with the observable capacitance and resistance of the system upon exclusion of the bulk resistance. Since $(C_0 - C_g)$ in the $(0, \infty)$ case is not, for $M \gg 1$, primarily associated with space charge but instead with diffusion and discharge, the present designation of Y_P, C_P, etc., as space-charge quantities is evidently not very appropriate in this case.

A common method of calculating the static or differential capacitance in a completely blocking linearized space-charge situation is to use $C_0 = C_{0E} \equiv (\epsilon/4\pi) \times (dE_1/dV_1)_0$, where the derivative has been evaluated at an electrode. For the $(0, 0)$ case, one finds $C_{0E} = rC_g$, in full agreement with the ac approach.[1] On the other hand, for $(0, \infty)$ $C_{0E} = [(r+1)/2]C_g$, again quite different from the ac C_0. It has already been mentioned[25] that the direct calculation of effective static capacitance in a situation with incompletely blocking electrodes is a difficult and apparently not entirely solved problem. The foregoing results illustrate the difficulty.

Although it is evidently impossible to obtain the operationally well-defined ac $(C_0 - C_g)$ from the present manipulations of the static space charge or surface field in a discharge situation, it is worth considering the operational situation which would be used to determine the static capacitance. Let us again consider applying a step function of voltage to the initially uncharged system. We shall assume that C_g and the parallel conductance branch, here $G_\infty/2$, have been measured and are known. The current associated with these elements can therefore be subtracted from the total charging current. Now if the remaining current, which flows in the Z_S branch for sinusoidal excitation, is integrated from $t = 0$ to ∞, one must obtain the total charge which can be stored in the system (exclusive of that in C_g). We have already seen from the earlier transient response calculation that this charge will be $(C_0 - C_g)V_0$, consistent with the ac $(C_0 - C_g)$ found for $\Omega \to 0$. This necessary agreement of ac and transient capacitances only holds for a linear system, where differential and "static" or integral capacitances are equal. For a non-

linear system the static and differential (or small-signal ac) capacitances are generally unequal.

The large low-frequency capacitance found in a discharge (or faradaic) situation is frequently termed a pseudocapacitance by electrochemists, presumably because it is associated with an electrode reaction. The present work has shown that this capacitance, (C_0-C_g), while perhaps strange in some of its aspects, is still a perfectly real capacitance associated with electrodes and the bulk of the material. I therefore believe pseudocapacitance is here somewhat of a misnomer. Further, our discharge boundary condition merely requires that the concentration of the discharging species remain unperturbed at the boundary of the system, an electrode. If the mobile, discharging species present in the material between electrodes is an electron, electrons merely need to pass freely into (and from) the electrode and from there into a current sink such as a signal generator or battery. It thus seems better to consider that the large (C_0-C_g) which appears is associated with a finite length l and with a certain boundary condition (or even an approximation to it) rather than always with a charge-transfer electrochemical reaction occurring at the electrode (hydrogen evolution, for example) or one in which the electrode material directly participates.

VII. APPLICATION TO ELECTROLYTE SITUATIONS

The present results have been derived for charge-containing material between two identical blocking or partly blocking plane, parallel electrodes separated by a distance l. Although this configuration corresponds to the usual situation for solid materials and such nearly insulating materials as liquid crystals, aqueous electrolyte and fused salt experiments are usually carried out differently. In addition to the electrode of major interest a counter, or auxiliary, electrode is employed whose interfacial impedance is negligible compared to that of the primary electrode. Such a counter electrode may be reversible (Ohmic, nonpolarizing, indifferent), or it may be of such great area compared to that of the main electrode that even though it is non-Ohmic its impedance is still negligible compared to other impedances present.

Now as we have seen in Fig. 17, independent of the blocking conditions at the two electrodes the positive and negative charge densities exhibit spatial antisymmetry around the center point at $x=l/2$. At this point, the original concentration c_0 of positive and negative carriers always remains undisturbed. It is thus possible in principle to put an Ohmic electrode at this position without changing anything. This electrode must be simultaneously Ohmic for charges of both signs; that is, it must function as a source or sink of charges of both signs. If half the original external voltage is applied between the electrode of interest and the Ohmic electrode, conditions in the region $0\leq x\leq l/2$ are the same as before. Thus, insofar as the counter electrode is a good approximation to Ohmic, the present results apply directly to the usual electrolyte situation with the transformation $l\rightarrow l/2$, $V_1\rightarrow V_1/2$. This doubles C_g and G_∞ because of their direct l dependence. In addition, the new (C_0-C_g) will be twice the old value in the $(0, 0)$ situation for $M\gg 1$ since in the two-blocking-electrode situation the two individual equal interface capacitances are in series. For the $(0, \infty)$ situation with $M\gg 1$, the above introduction of an Ohmic electrode at $x=l/2$ will halve (C_0-C_g) because of its direct proportionality to l in this case but the presence of capacitance at one electrode rather than two will restore (C_0-C_g) to its original value. For many of the normalized quantities of present interest, such as C_{SN} and R_{SiN}, the passage from two identical electrodes to one (working) electrode of interest and an indifferent electrode creates no change at all. For others, a simple transformation takes care of the matter. In the rest of this paper, we shall thus continue to use an electrode separation of l and the two identical-electrode results even for the electrolyte case.

When a much larger counter electrode is used than the primary electrode, the present expression for C_g will no longer apply and the actual C_g may be considerably larger than $\epsilon/4\pi l$. This is unimportant since C_g should be determined experimentally anyway. Note, however, that the area of the counter electrode cannot exceed that of the working electrode without either destroying the present one-dimensional character of the current flow or changing it from plane to cylindrical or spherical flow. Any of these changes would require changes in the present analysis.

In the electrolyte case, a common distinction is made between Faradaic and non-Faradaic processes. A Faradaic process is defined as one in which the amount of chemical reaction occurring is directly proportional to the amount of charge passed across the electrode boundary.[26] A typical non-Faradaic process is the charging of the double-layer capacitance of an ideal polarized electrode. While a Faradaic current involves an electrochemical reaction (and thus electron transfer), the present use of "discharge current" implies any kind of current (except displacement current) entering the electrode (together with an external circuit) as a sink for such current. When the current is carried by electrons both in the working material and the electrode, no electrochemical reaction need occur at the electrode. Thus, the present $(0, \infty)$ treatment is not limited to a Faradaic process for its discharge current. Nevertheless, in the present section, I shall be primarily concerned with discharging convection currents of ions (undergoing a charge-transfer reaction at an electrode), mass transfer via ions, and Faradaic currents.

Figure 18 shows three equivalent circuits which have been thought to be appropriate for the electrolyte situation with Faradaic current. Figure 18(a) follows from the present work and includes all the circuits of Figs. 5 and 10. For the $(0, 0)$ situation $R_F=\infty$ and $R_C=R_\infty$.

The frequency dependences of R_{Si} and C_S, which together form the impedance Z_i, have already been discussed. Alternatively, for the $(0, \infty)$ boundary condition, $R_F \equiv l/(\mu_n e c_0)$ and $R_C \equiv l/(\mu_p e c_0)$. The parallel combination of R_F and R_C is always R_∞, the solution resistance R_{sol}. Further, $R_{Si}+R_C \equiv R_S$. It seems quite clear that the general form of the Fig. 18(a) circuit should apply for $\mu_n \neq \mu_p$ as well as the present $\mu_n = \mu_p$ situation. It is not obvious, but seems probable to me, that it also applies as well for the general (r_p, r_n) discharge boundary condition after reinterpretation of the elements of the circuit.

Now since $|Z_i| \to 0$ as $\Omega \to \infty$, the $\Omega \to \infty$ limit of Fig. 18(a) is just C_g and R_∞ in parallel. Thus, measurement of the over-all admittance in the $\Omega \gtrsim 1$ range with extrapolation[27] to $\Omega = \infty$ should yield R_∞ and C_g from the extrapolated real and imaginary parts. The quantity C_g has almost always been ignored in electrolyte work; it clearly should not be for $\Omega \gtrsim 1$. It should be mentioned that the expression $G_\infty = (\mu_n+\mu_p) e c_0/l$ is only an approximation for usual cases of interest: high frequencies and nonzero concentrations.[28,29] Complications of this character will be ignored (as they usually are elsewhere) in the present idealized-model treatment.

It has already been implied that direct measurement of C_P and G_P in a parallel bridge arrangement will generally be impractical at such frequencies that $C_P \ll C_g$. For $M \gg 1$, the value of Ω for which $C_P = C_g$ is $M^{-1/2}$ for $(0, 0)$ and $(2M^2)^{-1/3}$ for $(0, \infty)$, both less than 0.1 for $M > 10^2$. The frequency range can be expanded to $\Omega \sim 1$ or more if bridge measurement can be made with a series arrangement. If the equivalent circuit is believed to be of the form of Fig. 18(a), the C_g and R_F elements should be determined separately (C_g in the absence of a discharging ion for example, and R_F as $\Omega \to 0$ or by transient response measurements) and then elements equal to them put in parallel with the R_S and C_S elements of the bridge, provided equal bridge arm ratios are employed. Then the R_S and C_S components of Z_S may be obtained at different frequencies directly from the balanced-bridge values.

Armstrong, Race, and Thirsk[30] have presented C_P and C_S values up to 400 kHz for $0.9M$ NaF in an essentially ideal polarized electrode situation. C_P showed ω^{-2} behavior and C_S remained constant to the maximum frequency. Although C_g was not stated, τ_D was probably no larger than $10^{-10}s$ here, and the maximum Ω achieved must have been much less than unity. The above authors give a careful discussion of problems of bridge measurement for electrolytes and suggest that above about 40 kHz a parallel rather than series bridge arrangement should be employed. Using small electrode areas and unequal bridge arm ratios, it may be possible, however, to use the series arrangement to much higher frequencies.

Many different equivalent circuits have been proposed when Faradaic and non-Faradaic processes are simultaneously present. Parsons[26] has recently reviewed them, with especial attention to the effects of adsorption of the reacting species on the electrode. Here we are only concerned with situations where such adsorption is absent. Thus, Figs. 18(b) and 18(c) show two circuits constructed to represent the situation without adsorption.

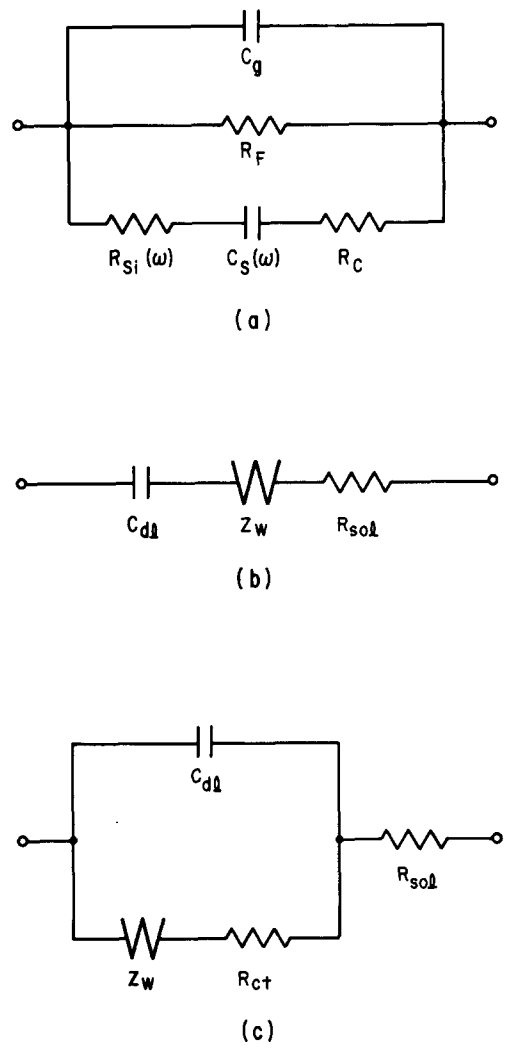

FIG. 18. Equivalent circuits for the electrolyte situation with discharge. (a) Following from present work; (b) Barker[31]; (c) conventional.

Figure 18(b) was suggested by Barker.[31] Although C_g is ignored, its absence is not serious for sufficiently low frequencies. More serious, however, is the simultaneous presence of both C_{dl} and Z_W. Here C_{dl} is defined as the zero-frequency double-layer differential capacitance and R_{sol} is the bulk solution resistance, R_∞. Now if C_W is the Warburg capacitance of Z_W, there is always a frequency below which the impedance of C_{dl} exceeds that of C_W; thus, as the circuit shows, the limiting low-frequency capacitance is indeed C_{dl}. Further, at sufficiently high frequencies, the impedance of C_{dl} is negligibly small compared to that of C_W. Thus, C_W is properly the high-frequency limiting capacitance.

There are at least two main reasons, however, why Fig. 18(b) is probably not entirely applicable in the situation where both Faradaic and non-Faradaic processes are simultaneously present. First, it includes a frequency-independent capacitance C_{dl}. But at sufficiently high frequencies, there will be no time to establish a space-charge region at an electrode during a half-cycle of the applied sinusoidal potential. Then if C_{dl} is associated with space charge, it does not exist, a stronger statement than to maintain that there is insufficient time to charge (or discharge) it. Certainly it seems valid to claim the nonexistence of C_{dl} for $\Omega \gg 1$, where as we have seen in the present $(0, \infty)$ treatment only the final Warburg diffusion capacitance still appears. Even the magnitude of the Warburg impedance in this region is generally very small compared to R_∞, however.

Second, we have seen in the $(0, \infty)$ situation that the double-layer capacitance, $(C_0 - C_g)$ at low frequencies, doesn't persist to the frequency range where a Warburg impedance appears. Instead, there is a smooth transition from one phenomenon, charging of the double-layer capacitance, to the other, diffusion-limited current and Warburg impedance. Thus, it appears improper in general for both C_{dl} and Z_W to be shown present for all frequencies.

The circuit of Fig. 18(c) has been widely used[13-16,32,33] for aqueous electrolytes and fused salts. Again no C_g appears while again a frequency-independent C_{dl} does. Here, however, the prescription to obtain C_{dl} is either to measure it in the absence of any discharge[26,32-35] or to obtain it by extrapolation to infinite frequency (provided $R_{ct} > 0$).[26,31,36,37] Here R_{ct} is the charge-transfer resistance arising from a finite exchange current; it is zero for a completely reversible electrode (infinite exchange current).

If the circuit of Fig. 18(c) were indeed appropriate and C_{dl} were frequency independent, then it would be proper to obtain C_{dl} by high-frequency extrapolation since $|Z_W| \to 0$ as the frequency is increased. Alternatively, if C_{dl} were unaffected by the presence or absence of a Faradaic current, it could most conveniently be obtained by measurement under conditions of no Faradaic process present. If the present $(0, \infty)$ results are at all applicable to the electrolyte situation, it appears that neither of the above possibilities is likely, and, in fact, that Fig. 18(c) is not an entirely appropriate equivalent circuit.

In early analyses of electrolyte experiments simultaneously involving both Faradaic and non-Faradaic processes, it was taken for granted that the processes didn't interact and that *a priori* separation was possible. Although Grahame[13] discussed qualitatively some interaction effects, it was only considerably later[26,36,37] that the theoretical and experimental study of interaction effects became popular. Even recently, Parsons[26] could state that few experiments had been undertaken to investigate such coupling effects. Finally, although the importance of coupling is still moot in general, De Levie and Husovsky[33] suggest that coupling can be ignored in the absence of specific adsorption. This matter will be further discussed later on.

The present $(0, \infty)$ idealized-model treatment is not a perfect exemplar of the usual electrolyte situation with discharge, which includes the presence of an indifferent electrolyte, but it clearly shows that in the absence of an indifferent electrolyte, discharge produces a profound effect, such that Faradaic and non-Faradaic processes are so coupled that they become almost indivisible parts of a single process. The effect of an indifferent electrolyte will be examined later.

The working-electrode boundary condition for the discharging species in the present $(0, \infty)$ treatment corresponds to that of a reversible or Ohmic electrode (for that species). If $0 < r_n < \infty$, so some discharge can still occur, we may expect the appearance of a charge-transfer resistance, as in Fig. 18(c). In the electrolyte case, R_{ct} is related to the rate constant of the surface reaction[15,32] and is frequency independent. To the degree that such a resistance would appear in a $(0, r_n)$ treatment with $r_n < \infty$, it seems necessary that it occur in series with the R_F of Fig. 18(a). Since R_F is a bulk resistance and R_{ct} a surface one, they could be distinguished, in principle, by their different dependence on applied potential and on electrode separation.

The attentive reader will have noted that only in the circuit of Fig. 18(a) is there a dc or static current path. None is present in the 18(c) circuit because the Warburg resistance, capacitance, and capacitative reactance approach infinity as $\omega \to 0$. Conditions for the maintenance of a continuous current are discussed by Grahame.[13] The present (r_p, r_n) boundary conditions allow a continuous current in response to a static applied voltage V_0 unless both r_p and r_n are zero. On the other hand, the usual electrolyte treatments[16,38,39] (both sinusoidal steady state and transient) allow a depletion of the concentration of the reacting ion at the electrode and a buildup of the product of the reaction. There is therefore no static current, and the transient current eventually falls to zero when the forward and reverse reaction rates become equal. In the present $(0, \infty)$ transient treatment there is a steady current $I_F \equiv V_0/R_F$ and a steadily decreasing current I_i which decreases to zero as $t \to \infty$ and the final $(C_0 - C_g)$ bulk capacitance is charged. Thus, the processes are quite different in general, although similarity may be expected for sufficiently short times that depletion and the back reaction remain unimportant.

Such similarity is indeed found in that both the present treatment [Eq. (22)] and electrolyte treatments for reversible processes[16,38,39] yield an initial current decay proportional to $t^{-1/2}$. Such behavior is frequently found experimentally whether there is or isn't a final static current. For example, Delahay[16] gives an experimental curve of current density vs $t^{1/2}$ which he fits approximately for short times by a current propor-

tional to $(1-at^{1/2})$, where a is a constant. Actually, the curve is closely proportional to $t^{-1/2}$ for the full time span given. Frequently plotting $t^{1/2}I$ rather than I alone will be useful to show any deviation from $t^{-1/2}$ behavior.

It is also worth mentioning that Raleigh and Crowe[40] have found charge results for transients in AgBr which show $t^{1/2}$ behavior over an appreciable span of time. Although these authors believe they have found ideal polarized electrode behavior with this system, their times were many orders of magnitude too long for their $q \propto t^{1/2}$ curve to have arisen from the (0, 0) final Warburg region, as in Fig. 9. As they suggest, their $t^{1/2}$ behavior is almost certainly associated with a Faradaic current, perhaps either electronic or from discharging impurity ions, as in Fig. 16. Here, of course, the time scale for $t^{1/2}$ response can extend to very long times for sufficiently large M.

Although both the conventional and present treatments yield $t^{-1/2}$ initial current behavior, the actual response is quite different in the two cases. We have seen that integration from $t=0$ to ∞ of I_i for both the (0, 0) and (0, ∞) cases leads to the necessary result $q_i(\infty)=(C_0-C_g)V_0$. On the other hand, although the conventional electrolyte treatments lead to continuously decreasing current–time curves which go to zero as $t\rightarrow\infty$, the total charge passed appears to be infinite. This result cannot be ascribed to current passing through a dc path, such as R_F of Fig. 18(a), since there is no such path present in these treatments. It can, however, be explained in terms of the way the Warburg impedance occurs in the conventional equations and in such circuits as Figs. 18(b) and 18(c).

All conventional electrolyte double-layer treatments of discharge implicitly or explicitly assume that everything interesting happens near the working electrode. Further, they ignore electromigration, assume electroneutrality,[41] and consequently solve ordinary diffusion equations with boundary conditions specified at the electrode ($x=0$) and at $x=\infty$. Thus, no finite l is even introduced. It is natural then to ignore C_g, although R_∞ or R_{so1} obtrudes and rarely can be ignored. The results of the present treatment come from an analysis in which electromigration is not ignored, electroneutrality is not assumed, and Poisson's equation holds exactly everywhere. Nevertheless, as might be expected we find that electroneutrality actually applies very well, as usual, everywhere except in the electrode interphase region.

The conventional treatments lead to a Warburg impedance which appear at all frequencies, as in Figs. 18(b) or 18(c). On the other hand, the present exact treatment of an idealized model with finite l leads, for (0, ∞), to two Warburg regions, both occurring only over limited frequency regions. The Warburg response which appears here for $(10/M)^2 \lesssim \Omega \lesssim 0.1$ may be associated with the conventional electrolyte treatment Warburg response. The reason why one appears over a limited frequency range and the other for all frequencies probably lies somewhat in the exact character of the present solution (no assumption of electroneutrality, etc.), but mostly in the finite l assumed in the present paper.

When a semi-infinite region is assumed, the diffusion region can grow arbitrarily large as the frequency becomes arbitrarily low. On the other hand, for finite l this region eventually becomes limited by l and the Warburg resistance and capacitance must cease increasing as the frequency decreases. As we have seen, the limiting response occurs for $\Omega \lesssim 10/M^2$. This condition[42a] corresponds to $(l/2) \lesssim 3l_d$; thus, (C_0-C_g) approaches close to its low-frequency limiting value when there are less than three diffusion lengths contained in $(l/2)$. The spreading of the diffusion region through all the length l at sufficiently low frequencies is, of course, the reason why R_{Si0} and (C_0-C_g) depend on l in the (0, ∞) case. In the absence of a discharge current, there is no coupling of what should be interface quantities to the entire bulk of the material and then R_{Si0} and (C_0-C_g) are independent of l. The presence of a Warburg impedance at all frequencies in the conventional treatments of the interface region with a Faradaic process present explains the infinite charge result mentioned above; it may be readily proved that the response of a Warburg impedance to a small step function of voltage involves a current whose integral over all time is infinite. Thus we see that whenever experimental frequencies or measuring times are sufficiently low or long $[\Omega<(10/M)^2]$, treatments such as the present (0, ∞) one with *finite* not infinite l are required.

It has become conventional in electrolyte work to plot R_{Si} and $(\omega C_S)^{-1}$ vs $\omega^{-1/2}$, as in Figs. 11 and 12 for the corresponding normalized quantities. When $R_{ct}\neq 0$, the $\omega\rightarrow\infty$ value of the series resistance (excluding the bulk resistance) is just R_{ct}; thus, in this case one obtains a straight line for the resistance lying above that for the capacitative reactance. Here, where $R_{ct}\equiv 0$, the lines coincide, as is often found experimentally.[32,42] Apparently, measurements have not been carried to sufficiently low frequencies that the separation between the lines, as in the right of Fig. 12, shows up clearly. It is, of course, also obvious that analysis of experimental results in terms of the wrong equivalent circuit [say that of Fig. 18(c) instead of that of 18(a) if the latter is the proper one in a given situation] can lead to improper deductions about various elements of the equivalent circuit and about their frequency dependence.

In electrolyte solutions, it is usually found that the over-all low-frequency limiting capacitance of an ideally polarized electrode without specific adsorption is largely determined by the capacitance C_1 of a "charge-free" layer next to the electrode, rather than the present (0, 0) space-charge (diffuse layer) capacitance $(C_0-C_g)\equiv s_bC_g$. This inner layer capacitance is thought to arise from the presence of a monolayer or so of solvent between the electrode and the rest of the solution.[43–47] The capacitance of the layer depends only weakly on the potential difference across it and generally falls in

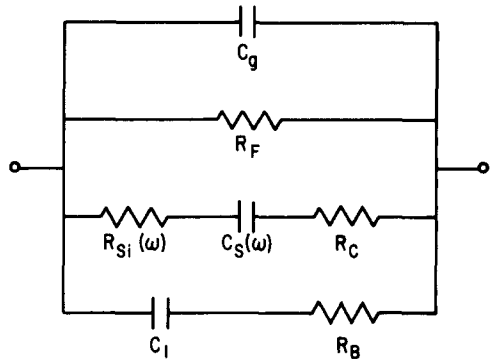

FIG. 19. Approximate (uncoupled) equivalent circuit for the $(0, \infty)$ discharge case when an excess of indifferent electrolyte is present.

the range of 15–45 μF/cm^2. Somewhat similar insulating or charge-depleted layers next to an electrode have frequently been suggested for the electrode–solid material situation as well.[24,48–53]

When the concentration c_0 is high and/or when the potential difference between the electrode and the bulk of the material appreciably exceeds kT/e in magnitude, s_bC_g will be much larger than 45 μF/cm^2. Then, the series combination of C_1 and s_bC_g will be dominated by C_1, a capacitance essentially independent of frequency until at least the high microwave range.[47] Under these conditions, the (0, 0) equivalent circuit of Fig. 5(a) will still be applicable if the capacitance s_bC_g is replaced by C_1. It should be mentioned, however, that the eventual high-frequency Warburg, or diffusion-effect, reduction of C_S will cause C_1 to no longer dominate the series combination of C_1 and C_S at some high relative frequency. For example, the admittances of C_1 and C_S are equal for the (0, 0) case at $\Omega=2(MC_g/C_1)^2$. Above this frequency, the admittance of the diffusion capacitance is the smaller, and it then begins to dominate the series combination. Thus, even in this case, it appears to be improper to obtain the double-layer capacitance [regarded as C_1, (C_0-C_g), or, properly, their series combination] which is expected to apply at low relative frequencies from capacitance measurements extrapolated to infinite frequency in the usual way.

When a Faradaic process is present, it is frequently found that the measured series capacitance at low frequencies is of the order of 10^3–10^4 μF/cm^2, far larger than C_1. It is thus evident that C_1 cannot be in series with (C_0-C_g) in the discharge case but that it is effectively bypassed by the Faradaic current path. Physically, discharge cannot occur without charge carriers passing through the inner layer, probably displacing adsorbed solvent molecules as they do so. It thus appears that in the general (r_p, r_n) discharge case (r_p and r_n not simultaneously zero), C_1 is of negligible importance and may usually be ignored.

The treatment and discussion thus far have applied to a situation where positive and negative charge carriers having a common equilibrium concentration, c_0, are simultaneously present. This assumption corresponds to the usual (0, 0) ideal polarized electrode electrolyte situation (e.g., NaF in water with a dropping mercury electrode) and to the preferred condition for conduction experiments in solids. On the other hand, it is customary, when an electrolytic Faradaic process is under investigation to add a high concentration, say c_1, of indifferent electrolyte. For simplicity, here and in the rest of the paper, I assume univalent ions only present. The indifferent solute is chosen to dissociate into ions for which the working electrode is blocking, or ideally polarized, over the entire range of applied potentials of interest. The high c_1 reduces L_D, increases M, and reduces the associated solution resistance R_∞, which we shall here term R_B. In the absence of discharge, the present (0, 0) treatment should apply to these ions. The large c_1 and corresponding large s_bC_g virtually ensure that for all conditions of interest the series combination of C_S and C_1 is essentially C_1. Further, the small R_B (frequently as low as 10–100 $\Omega\cdot$cm^2) causes the $\Omega=1$ point to occur at an actual frequency beyond the usual limit of measurement (say $>10^7$ MHz).

We see that if there were no coupling here between the c_0 Faradaic and the c_1 non-Faradaic processes, the presence of a high concentration of indifferent electrolyte would add an additional parallel admittance to the circuit of Fig. 18(a), consisting essentially of C_1 in series with the small resistance R_B. These elements would remain frequency independent over the entire range of measurement. The resulting equivalent circuit is shown in Fig. 19. Although Faradaic and non-Faradaic processes are coupled by Poisson's equation, nonnegligible in the neighborhood of an electrode, the circuit of Fig. 19 may be useful under some conditions, and its implications will be discussed below. Its range of validity could be assessed by a detailed space-charge treatment of the present type in which four species of ions of any valence were simultaneously present: blocked positive and negative ions of equilibrium concentration c_1, and different positive and negative ions of equilibrium concentration c_0 (usually $c_0 \ll c_1$) having discharge parameters of r_p and r_n (with r_p and r_n not simultaneously zero).

The Fig. 19 over-all equivalent circuit arrived at above differs from the conventional one of Fig. 18(c) in two minor and two major ways. The minor differences are the presence of C_g and the absence of R_{ct}. Clearly C_g should be included if measurements extend to sufficiently high frequencies that the reactance of C_g becomes comparable to the magnitude of the impedance of any of the three remaining parallel branches. Although R_{ct} is overtly omitted, it can be included when appropriate in the R_F branch as discussed earlier. Note that in the present uncoupled approximation changes in c_1, and thus in R_B, do not affect R_F and R_C at all. Further it should be noted that although the entire

equivalent circuit of Fig. 19 can be formally represented by a noninfinite capacitor and resistor in series or in parallel, the frequency dependences of the resulting elements would be very much greater than those of the elements shown in Fig. 19 and the physical interpretation of the new elements would be opaque.

One of the major differences arises from the present finite-length approach, consistent with the finite length actually employed in any experiment. This approach leads not to the conventional Warburg resistance and capacitance that indefinitely increase as the frequency decreases but to elements which reach limiting values depending on l for sufficiently low frequency.

Second, there is a most significant difference in the way the resistances enter. The bulk or solution resistance has conventionally been operationally defined as the limiting high-frequency resistance. In Fig. 19 this resistance, applicable at frequencies where the capacitative reactances of C_1 and C_S are much smaller than the resistances in series with them, is clearly made up of the parallel combination of R_F, R_C, and R_B. Thus when all valences are equal to one, $R_{sol}=[(\mu_{n_0}ec_0/l)+(\mu_{p_0}ec_0/l)+(\mu_{n_1}+\mu_{p_1})(ec_1/l)]^{-1}$, where the "0" and "1" mobility subscripts associate ionic mobilities with their corresponding equilibrium concentrations. Assuming reasonable mobilities and $c_1 \gg c_0$, one finds $R_{sol} \cong R_B$. In fact, some of the main reasons for the use of a high-concentration indifferent electrolyte have been to minimize electromigration and to reduce R_{sol}, thereby hopefully allowing R_{ct} and other element values to be more accurately determined. Further, in order to determine $R_B \cong R_{sol}$, one need not go to such high frequencies that $\Omega \gg 1$ (here Ω should be calculated using c_1), but only to the region where $\omega R_B C_1 \gg 1$, a condition usually satisfied at a much lower frequency.

The resistance R_{sol} is in series with everything else in Fig. 18(c) while $R_B \cong R_{sol}$ is only in series with C_1 in Fig. 19. This difference can lead to appreciable difference over-all response and again suggests that elements derived from assuming the applicability of the conventional circuit when the present over-all one is really appropriate can be appreciably in error in parts of the frequency range.

If we identify the present C_1 with the C_{dl} of Fig. 18(c), then we may compare the C_{dl} and R_{sol} of 18(c) with C_1 and R_B of the present approximate circuit. If $(\omega C_1)^{-1}$ were small compared to the magnitudes of the impedances of the other three parallel branches of the over-all circuit, then $Z_B \equiv R_B+(i\omega C_1)^{-1}$ would be the dominant or main current-carrying branch and the Faradaic elements only a small perturbation to the over-all situation. Now although R_B may be made much smaller than R_C, the inner layer capacitance C_1 will generally be far smaller than C_S at low frequencies. Thus both the C_S and C_1 branches must usually be considered simultaneously over a considerable frequency span.

In the region where $\omega R_B C_1 \ll 1$, R_B may be neglected compared to $(\omega C_1)^{-1}$. Then, C_1 appears exactly as does the C_{dl} of Fig. 18(c), in parallel with everything. It may then be a temptation to put R_B in series with everything, as in Fig. 18(c), but, as we have seen, this would indeed be a poor approximation. It may be a poor approximation even when c_0-c_1 coupling is properly taken into account. Finally, note that when $R_F \gg R_B$, as is usually the case, it will be very easy for the experimenter to ignore or forget about its existence unless measurements are extended to sufficiently low frequencies that R_F becomes the dominant resistance of the equivalent circuit.

Note that if complete decoupling between the effects of the c_0 and c_1 type ions is a good approximation and thus the circuit of Fig. 19 is applicable, adding the c_1 indifferent or supporting electrolyte merely complicates the determination of the Faradaic process elements, rather than aids their determination as has been commonly expected. In actual fact, however, a high-concentration indifferent electrolyte decouples from each other the positive and negative charges of lower concentration c_0 and greatly reduces their electromigration. Their effects can then be considered independently of each other. It is important to emphasize, however, that even in an exact solution of the problem the magnitude of c_1 cannot influence R_F since this frequency-independent resistance provides a dc path and the c_1 ions, being blocked, cannot contribute to such a path. On the other hand, an exact solution, which would include any coupling effects in the space-charge region next to the working electrode, would almost certainly lead to some dependence of R_C and the other elements in this branch on c_1 if the present circuit geometry and structure even remained applicable.

In the present treatment, the applied sinusoidal potential amplitude V_1 or the transient potential V_0 has been assumed much less than kT/e in magnitude and has also been assumed to be a small perturbation to the equilibrium condition of the system where the concentration c_0 (and/or c_1) is constant for all x. In the electrolyte situation this equilibrium condition corresponds to the point of zero (electrode) charge (p.z.c.). For the semiconductor case it is the flat-band condition.

In electrolyte double-layer experiments, a static bias potential is usually applied as well as a small alternating V_1 or transient V_0. Let us reference this bias potential to the p.z.c. and designate it as Ψ_0. Now $|\Psi_0|$ may greatly exceed kT/e and thus perturb the static or equilibrium concentrations of the charge carriers so that they are far from homogeneous. In a completely blocking case, the presence of $|\Psi_0| > kT/e$ will lead to an equilibrium condition in which anions concentrate at the anode and cations at the cathode. The small V_1 or V_0 then represents a very small perturbation to this new equilibrium. In a discharge case, Ψ_0 will, of course, lead to a continuous discharge current and may again greatly perturb the steady state distribution of the various charge carriers present.

In either a blocking or discharge case, the system

responds nonlinearly to Ψ_0 when the magnitude of this potential is comparable to or greater than kT/e. But although the system is then nonlinear, V_1 or V_0, if their magnitudes are much smaller than kT/e, "feel" only the locally linear system. In essence, although all the parameters of the system may depend nonlinearly on Ψ_0, at a given fixed Ψ_0 one can measure the parameter values associated with this Ψ_0 in a linear fashion. The resulting parameter values are those of the linear system which represents the response of the actual nonlinear system for infinitesimal perturbations about a given state.

We may thus obtain resistance and capacitance values and impedances for any Ψ_0. The function of Ψ_0 is then to shift the system from one set of values to another. It is fortunate that we can use a linear approach in this way since the whole concept of impedance (more generally, immittance), in its usual formulation, is a child of linearity. Of course, these considerations mean that although a given equivalent circuit structure may apply unchanged over a considerable range of Ψ_0, at constant frequency there are different values of its capacitative and resistive elements for every different Ψ_0.

The present $(0, 0)$ and $(0, \infty)$ results apply exactly only for $\Psi_0=0$. I know of only one approximate computer calculation of space-charge frequency response where the equilibrium charge carrier distribution was perturbed and not taken homogeneous.[53] This treatment unfortunately does not apply to the present situation but was concerned with a space charge of negative vacancies in a solid having no compensating charge of opposite sign. Clearly, in order to carry out a proper frequency response calculation for the present system when $\Psi_0\neq 0$, one would first require a static solution, such as that of Ref. 54 for the $(0, 0)$ case or one similar to the dc solution of Ref. 25 in a continuous-current discharge situation. Then, perturbations from this solution arising from a small applied sinusoidal potential would be calculated to obtain the resulting alternating current, impedances, and equivalent circuit elements.[53]

The space-charge explanation of large measured capacitances in electrode-solid situations has sometimes been doubted[55] because experiments frequently show little or no dependence of capacitance on applied voltage amplitude over a range much larger than kT/e. At least part of such independence may arise from the presence of a charge-free inner molecular layer in an electrolyte and/or a depletion or exhaustion layer next to the electrode abutting a solid. Such a layer may arise from many causes; sometimes, for example, from the "built-in" or diffusion potential associated with the electrode-solid contact.[25,53] If this potential is large compared to any applied sinusoidally varying potential, the amplitude of the latter shouldn't affect the measured capacitance which, in turn, would be largely determined by the thickness of this region rather than by an accumulation of space charge near the electrode. Further, in a discharge case such as $(0, \infty)$, it may turn out that the ac (C_0-C_g), which, as we have seen, isn't primarily a space-charge capacitance, is considerably less dependent on Ψ_0 than the space-charge capacitance of the $(0, 0)$ situation.

In the electrolyte case, it is generally found that no Faradaic discharge of a particular ion occurs until Ψ_0 reaches a certain value, the potential step for the actual charge transfer reaction which takes place. The discharge parameters and boundary conditions for the various ions present are thus generally very potential dependent. In the present treatment we have implicitly taken $\Psi_0=0$ and have thus not needed to consider any change of the boundary conditions with Ψ_0, such as potential dependence of r_p and r_n. Nevertheless, it seems likely that the present $(0, 0)$ and $(0, \infty)$ treatments, idealized as they are, should apply sufficiently to the real $\Psi_0\neq 0$ electrolyte situation that at least the structure of the present equivalent circuits (and perhaps much of the frequency dependence of the R_{Si} and C_S elements) should be at least somewhat applicable.

Although the present $(0, 0)$ and $(0, \infty)$ analyses are the most detailed and exact ones worked out thus far, the time seems ripe for following the same detailed microscopic approach without some of the present idealizations such as $\Psi_0=0$, no indifferent electrolyte, etc. Although an exact treatment of the $\Psi_0\neq 0$ discharge case with an excess of indifferent electrolyte present would require computer solution, its results could prove most worthwhile. The sinusoidal-response part of such a calculation should not be attempted, however, until a static or transient solution is obtained which holds over a range of Ψ_0 and yields good agreement with experiment. To achieve such agreement may require boundary conditions both sensitively dependent on Ψ_0 and different from those considered here for $\Psi_0=0$ and previously for $\Psi_0\neq 0$.

VIII. SYMBOL GLOSSARY

C_g	Geometric capacitance/unit area, $\epsilon/4\pi l$
C_{dl}	Double-layer capacitance/unit area
C_{iP}	Capacitative component of the "interface" admittance/unit area, Y_i. $C_{iPN}\equiv C_{iP}/(C_0-C_g)$
C_P	Parallel space-charge capacitance/unit area. $C_{PN}\equiv C_P/(C_0-C_g)\equiv s^{-1}(C_P/C_g)$
C_S	Series space-charge capacitance/unit area. $C_{SN}\equiv C_S/(C_0-C_g)\equiv s^{-1}(C_S/C_g)$
C_{SC0}	Static space-charge capacitance/unit area obtained from ρ_1
C_0	Low-frequency limiting value of C_P, C_S, and C_{iP}, all plus C_g
C_{0E}	Static capacitance/unit area calculated using E_1
C_1	Capacitance/unit area of the inner, "charge-free" layer abutting an electrode

D_n, D_p	Diffusion coefficients of the negative and positive charge carriers
E_1	Amplitude of the fundamental component of the electric field
G_{iP}	Conductive component of the "interface" admittance/unit area Y_i
G_P	Parallel space-charge conductance/unit area. $G_{PN} \equiv G_P/G_\infty$ [blocking case]; $G_P/(\frac{1}{2}G_\infty)$ [discharge case]
G_S	Series space-charge conductance/unit area. $G_{SN} \equiv G_S/G_\infty$ [blocking case]; $G_S/(\frac{1}{2}G_\infty)$ [discharge case]
G_0	Low-frequency limiting value of G_S. $G_{0N} \equiv (s_b^2/\Lambda_b)$ [blocking]; $(4s_d^2/\Lambda_d)$ [discharge]
G_∞	Bulk conductance/unit area. High-frequency limiting value of G_P and G_S, σ_∞/l
$I_i(t)$	Current/unit area associated with the "interface" region, or admittance/unit area Y_i, upon application of a voltage step. $I_{iN} \equiv \tau_D I_i/(C_0-C_g)V_0$
L_D	Debye length, $[\epsilon kT/8\pi e^2 c_0]^{1/2}$
M	$l/2L_D$
R_B	Series resistance-unit area associated with the indifferent electrolyte (Fig. 19)
R_C	Frequency-independent series resistance-unit area associated with C_S for the $(0, 0)$ or $(0, \infty)$ cases
R_F	Frequency-independent bridging resistance-unit area associated with continuous discharge in the $(0, \infty)$ case
R_S	G_S^{-1}. $R_{SN} \equiv G_{SN}^{-1}$
R_{Si}	$R_S - R_\infty$ [blocking]; $R_S - 2R_\infty$ [discharge]
R_{Si0}	Low-frequency limiting value of R_{Si}
R_{sol}	Electrolyte solution resistance-unit area
R_0	G_0^{-1}; $R_{Si0}+R_\infty$ [blocking]; $R_{Si0}+2R_\infty$ [discharge]
R_∞	G_∞^{-1}
T	Absolute temperature
T_i	$(2M^2\Omega)^{1/2}R_{SiN}$ [$(0, \infty)$ case]
U_i	$(2M^2\Omega)^{1/2}(2s_d\Omega C_S)^{-1}$ [$(0, \infty)$ case]
V_0	Amplitude of applied step voltage
V_1	Amplitude of sinusoidal applied voltage. $V_1^* \equiv eV_1/kT$
W	$(2x/l)-1$
Y_C	$(\mu_n e c_0/l)+i\omega C_g$ [$(0, \infty)$ case]
Y_i	Z_i^{-1}. $Y_{iN} \equiv Y_i/G_\infty$ [blocking], $Y_i/(\frac{1}{2}G_\infty)$ [discharge]
Y_P	Space-charge admittance/unit area, $G_P+i\omega C_P$. $Y_{PN} \equiv Y_P/G_\infty$ [blocking]; $Y_P/(\frac{1}{2}G_\infty)$ [discharge]
Y_T	Y_C+Y_P [$(0, \infty)$ case]
Y_W	Z_W^{-1}. $(\omega)^{1/2}(1+i)/2\eta$
Z_i	$Z_S - R_\infty$ [blocking]; $Z_S - 2R_\infty$ [discharge]
Z_S	Y_P^{-1}. $R_S+(i\omega C_S)^{-1}$
Z_W	Warburg impedance-unit area, $\eta(1-i)/(\omega)^{1/2}$
Z_{W_b}	Warburg impedance-unit area in blocking case, $(iM^2\Omega)^{-1/2}R_\infty$
Zw_{d_1}	Warburg impedance-unit area in discharge case for $(10/M)^2 \lesssim \Omega \lesssim 0.1$, $(iM^2\Omega)^{-1/2}(4R_\infty)$
Zw_{d_2}	Warburg impedance-unit area in discharge case for $\Omega \gg 1$, $(iM^2\Omega)^{-1/2}(2R_\infty)$
c_0	Equilibrium homogeneous concentration of positive and negative charge carriers in the $(0, 0)$ and $(0, \infty)$ cases
c_1	Equilibrium homogeneous concentration of positive and negative charge carriers of the indifferent electrolyte
e	Protonic charge
k	Boltzmann's constant
l	Distance of separation of two plane, parallel electrodes
l_d	Diffusion length, $(D_n/\omega)^{1/2}$
n_1	Amplitude of the fundamental component of the negative charge concentration. $n_1^* \equiv n_1/c_0V_1^*$
p	Laplace transform complex frequency variable. Also used as concentration of positive charge carriers
p_1	Amplitude of fundamental component of the positive charge concentration. $p_1^* \equiv p_1/c_0V_1^*$
$q_i(t)$	Charge/unit area associated with the "interface" region, or admittance/unit area Y_i, upon application of a voltage step. $q_{iN} \equiv q_i/(C_0-C_g)V_0$
r	M ctnh(M)
r_n, r_p	Blocking or discharge parameters for n_1 and p_1 at an electrode
s	$(C_0-C_g)/C_g$. $s_b \equiv (r-1)$ and s_d [see Eq. (5)] are blocking and discharge case expressions for s
t	Time
x	Distance measured from left electrode
Λ_b, Λ_d	Low-frequency limiting value of G_{PN}/Ω^2 for blocking and discharge situations
Ω	Normalized radial frequency, $\omega\tau_D$ and $[L_D/l_d]^2$
Ψ_0	Static applied potential
ϵ	Dielectric constant of the charge-containing medium
η	A parameter in the Warburg impedance-unit area
μ_n, μ_p	Mobilities of the negative and positive charge carriers
ρ_1	Space-charge density, $e(p_1-n_1)$
σ_∞	High-frequency limiting conductivity, $ec_o(\mu_n+\mu_p)$
τ_D	Dielectric relaxation time, $C_g/G_\infty \equiv C_g R_\infty = \epsilon/4\pi\sigma_\infty$
ω	Radial frequency, $2\pi f$, of the applied sinusoidal voltage

ACKNOWLEDGMENTS

It is a pleasure to thank D. R. Powell for the computer programming involved in this work and C. A.

Barlow, Jr. and E. L. Jones for their valuable comments and suggestions.

[1] J. R. Macdonald, Phys. Rev. **92,** 4 (1953).
[2] R. J. Friauf, J. Chem. Phys. **22,** 1329 (1954).
[3] H. Chang and G. Jaffé, J. Chem. Phys. **20,** 1071 (1952).
[4] J. H. Beaumont and P. W. M. Jacobs, J. Phys. Chem. Solids **28,** 657 (1967).
[5] J. R. Macdonald, Phys. Rev. **91,** 412 (1953).
[6] A. R. Allnatt and P. W. M. Jacobs, J. Phys. Chem. Solids **19,** 281 (1961).
[7] P. W. M. Jacobs and J. N. Maycock, J. Chem. Phys. **39,** 757 (1963).
[8] B. J. H. Jackson and D. A. Young, Trans. Faraday Soc. **63,** 2246 (1967).
[9] A. D. Franklin, S. Marzullo, and J. B. Wachtman, Jr., J. Res. Natl. Bur. Std. **A71,** 355 (1967).
[10] J. R. Macdonald, Trans. Faraday Soc. **66,** 943 (1970). In this paper the present parameter Ω is termed y and the present Q is denoted by Z. The reference to Eq. (17) on p. 956 should be to Eq. (16).
[11] E. Warburg, Wied. Ann. **67,** 493 (1899).
[12] F. Krüger, Z. Physik. Chem. **45,** 1 (1903).
[13] D. C. Grahame, J. Electrochem. Soc. **99,** 370C (1952).
[14] B. E. Conway, *Theory and Principles of Electrode Processes* (Ronald, New York, 1965).
[15] R. De Levie, Electrochim. Acta **10,** 395 (1965).
[16] P. Delahay, in *Advances in Electrochemistry and Electrochemical Engineering,* edited by P. Delahay (Interscience, New York, 1961), Vol. 1, pp. 233–318; see especially pp. 247–254.
[17] J. R. Macdonald and M. K. Brachman, Rev. Mod. Phys. **28,** 393 (1956).
[18] J. R. Macdonald and C. A. Barlow, Jr., Rev. Mod. Phys. **35,** 940 (1963).
[19] J. R. Macdonald, J. Appl. Phys. **34,** 538 (1963).
[20] R. Solomon, A. Sher, and M. W. Muller, J. Appl. Phys. **37,** 3427 (1966).
[21] K. S. Cole and R. H. Cole, J. Chem. Phys. **9,** 341 (1941).
[22] D. W. Davidson and R. H. Cole, J. Chem. Phys. **18,** 1417 (1950); **19,** 1484 (1951).
[23] S. H. Glarum, J. Chem. Phys. **33,** 639 (1960)
[23a] *Note added in Proof*: D. O. Raleigh has recently pointed out to me that E. H. Snow, A. S. Grove, B. E. Deal, and C. T. Sah [J. Appl. Phys. **36,** 1664 (1965)] have observed charge curves arising from ionic motion in an oxide film similar to those of Fig. 16. Only positive ions were of importance, however; the initial charge distribution was different from that considered here, and $|eV_0/kT| \gg 1$.
[24] J. R. Macdonald, J. Chem. Phys. **23,** 275 (1955).
[25] J. R. Macdonald, Solid State Electron. **5,** 11 (1962).
[26] R. Parsons, in *Advances in Electrochemistry and Electrochemical Engineering,* edited by P. Delahay (Interscience, New York, 1970), Vol. 7, pp. 177–219.
[27] R. P. T. Tomkins, G. J. Janz, and E. Andalaft, J. Electrochem. Soc. **117,** 906 (1970).
[28] A. Z. Borucka, J. O'M. Bockris, and J. A. Kitchener, Proc. Roy. Soc. (London) **A241,** 554 (1957).
[29] S. Glasstone, *Textbook of Physical Chemistry* (Van Nostrand, New York, 1950), 2nd ed., pp. 903–908.
[30] R. D. Armstrong, W. P. Race, and H. R. Thirsk, Electrochim. Acta **13,** 215 (1968).
[31] G. C. Barker, J. Electroanal. Chem. **12,** 495 (1966); Pure Appl. Chem. **15,** 239 (1967).
[32] J. E. B. Randles, Discussions Faraday Soc. **1,** 11 (1947).
[33] G. J. Hills and P. D. Power, Trans. Faraday Soc. **64,** 1629 (1968).
[34] R. De Levie and A. A. Husovsky, J. Electroanal. Chem. **22,** 29 (1969).
[35] R. D. Armstrong, D. F. Porter, and H. R. Thirsk, J. Electroanal. Chem. **14,** 17 (1967).
[36] P. Delahay, J. Phys. Chem. **70,** 2373 (1966).
[37] P. Delahay and G. G. Susbielles, J. Phys. Chem. **70,** 3150 (1966).
[38] K. Holub, J. Electroanal. Chem. **17,** 277 (1968).
[39] G. G. Susbielles and P. Delahay, J. Electroanal. Chem. **17,** 289 (1968).
[40] D. O. Raleigh and H. R. Crowe, Solid State Commun. **8,** 955 (1970); J. Electrochem. Soc. (to be published).
[41] J. Newman, in *Advances in Electrochemistry and Electrochemical Engineering,* edited by C. W. Tobias (Interscience, New York, 1967), Vol. 5, pp. 87–136.
[42] R. D. Armstrong, W. P. Race, and H. R. Thirsk, J. Electroanal. Chem. **14,** 143 (1967).
[42a] *Note added in proof*: R. D. Armstrong has recently pointed out to me that J. H. Sluyters [Rec. Trav. Chim. **82,** 100 (1963)] has obtained a very similar condition for the present case of two plane–parallel electrodes. His treatment involves the solution of simple diffusion equations for the ions of a redox couple. Thus, Poisson's equation does not hold exactly, electromigration, cell resistance, and geometrical capactitance are ignored, and the results apply most closely to a galvanic cell containing an excess of indifferent electrolyte. Sluyters investigates such a cell, concentrates attention on the dependence of the total impedance upon electrode spacing at a fixed applied frequency, and finds good qualitative agreement between theory and experiment as the spacing approaches zero. A paper comparing in detail his results and those herein will appear in J. Electroanal. Chem.
[43] J. R. Macdonald, J. Chem. Phys. **22,** 763, 1471, 1857 (1954).
[44] D. C. Grahame, J. Am. Chem. Soc. **79,** 2093 (1957).
[45] J. R. Macdonald and C. A. Barlow, Jr., J. Chem. Phys. **36,** 3062 (1962).
[46] J. R. Macdonald and C. A. Barlow, Jr., Proc. Australian Conf. Electrochem. 1st, 199 (1965).
[47] C. A. Barlow, Jr. and J. R. Macdonald, in *Advances in Electrochemistry and Electrochemical Engineering,* edited by P. Delahay (Interscience, New York, 1967), Vol. 6, pp. 1–199.
[48] J. R. Macdonald, J. Chem. Phys. **29,** 1346 (1958).
[49] J. R. Macdonald, J. Phys. Chem. Solids **21,** 313 (1961).
[50] J. M. Wimmer, J. Appl. Phys. **37,** 3728 (1966).
[51] A. Kessler and E. Mariani, J. Phys. Chem. Solids **29,** 1079 (1968).
[52] D. Miliotis and D. N. Yoon, J. Phys. Chem. Solids **30,** 1241 (1969).
[53] H. A. Hoyen, J. A. Strozier, Jr., and Che-Yu Li, Surface Sci. **20,** 258 (1970).
[54] J. R. Macdonald, J. Chem. Phys. **22,** 1317 (1954).
[55] P. H. Sutter and A. S. Nowick, J. Appl. Phys. **34,** 734 (1963).